Two Extratropical Pathways to Forcing Tropical Convective Disturbances

YUAN-MING CHENG,[a] STEFAN TULICH,[b] GEORGE N. KILADIS,[a] AND JULIANA DIAS[a]

[a] *NOAA/Physical Sciences Laboratory, Boulder, Colorado*
[b] *CIRES, University of Colorado and NOAA/Physical Sciences Laboratory, Boulder, Colorado*

(Manuscript received 22 March 2021, in final form 9 June 2022)

ABSTRACT: Observational evidence of two extratropical pathways to forcing tropical convective disturbances is documented through a statistical analysis of satellite-derived OLR and ERA5 reanalysis. The forcing mechanism and the resulting disturbances are found to strongly depend on the structure of the background zonal wind. Although Rossby wave propagation is prohibited in easterlies, modeling studies have shown that extratropical forcing can still excite equatorial waves through resonance between the tropics and extratropics. Here this "remote" forcing pathway is investigated for the first time in the context of convectively coupled Kelvin waves over the tropical Pacific during northern summer. The extratropical forcing is manifested by eddy momentum flux convergence that arises when extratropical eddies propagate into the subtropics and encounter their critical line. This nonlinear forcing has similar wavenumbers and frequencies with Kelvin waves and excites them by projecting onto their meridional eigenstructure in zonal wind, as a form of resonance. This resonance is also evidenced by a momentum budget analysis, which reveals the nonlinear forcing term is essential for maintenance of the waves, while the remaining linear terms are essential for propagation. In contrast, the "local" pathway of extratropical forcing entails the presence of a westerly duct during northern winter that permits Rossby waves to propagate into the equatorial east Pacific, while precluding any sort of resonance with Kelvin waves due to Doppler shifting effects. The intruding disturbances primarily excite tropical "cloud plumes" through quasigeostrophic forcing, while maintaining their extratropical nature. This study demonstrates the multiple roles of the extratropics in forcing in tropical circulations and illuminates how tropical–extratropical interactions and extratropical basic states can provide be a source of predictability at the S2S time scale.

SIGNIFICANCE STATEMENT: This study seeks to understand how circulations in the midlatitudes excite the weather systems in the tropics. Results show that the mechanisms, as well as the types of tropical weather systems excited, are strongly dependent on the mean large-scale wind structure. In particular, when the large-scale wind blows from east to west, a special type of eastward-moving tropical weather system, the Kelvin wave, is excited owing to its resonance with remote eastward-moving weather systems in the extratropics. On the contrary, when the average wind blows from west to east, midlatitude systems are observed to intrude into the lower latitudes and directly force tropical convection, the cloud plumes, while maintaining their extratropical nature. These results speak to how the midlatitudes can excite distinct types of tropical weather systems under different climatological wind regimes. Understanding these tropical weather systems and their interactions with the midlatitudes may ultimately help to improve predictions of weather beyond 2 weeks.

KEYWORDS: Kelvin waves; Tropical variability; Rossby waves; Dynamics; Atmospheric waves; Atmospheric circulation

1. Introduction

Tropical convection is often organized into synoptic-scale disturbances moving parallel to the equator that can be tracked for days or even weeks. These moist wavelike disturbances, which occur at higher frequencies than the Madden–Julian oscillation (MJO), include convectively coupled Kelvin waves (hereafter simply Kelvin waves), equatorial Rossby, mixed Rossby–gravity, inertio-gravity, and easterly waves. Together they explain a substantial fraction of rainfall variability in the tropics (Kiladis et al. 2009) and their passage can lead to severe weather, including extreme precipitation (Baranowski et al. 2020; Latos et al. 2021) and tropical cyclogenesis (Ventrice et al. 2012). They are also of interest owing to their potential to act as sources of subseasonal predictability that can ultimately extend from the tropics to extratropics, via Rossby wave teleconnections (e.g., Stan et al. 2017; Ying and Zhang 2017; Dias et al. 2018; Judt 2020; Dias et al. 2021). While it is now established that many of these disturbances can indeed be forced by extratropical Rossby waves (e.g., Zangvil and Yanai 1980; Yanai and Lu 1983; Liebmann and Hartmann 1984; Magana and Yanai 1995; Hoskins and Yang 2000; Yang and Hoskins 2013, 2016; Sakaeda and Roundy 2014, 2015, 2016; Yang et al. 2018; Cheng et al. 2019; Mayta et al. 2021; Kiladis 1998, hereafter K98; Straub and Kiladis 2003a, hereafter SK03; Huaman et al. 2020, hereafter HSK20; Tulich and Kiladis 2021, hereafter TK21), the precise mechanisms of this forcing have yet to be fully established. In this study, observational evidence is presented for two different extratropical forcing pathways to convective disturbances over the tropical Pacific, whose relative contributions are strongly dependent on the meridional structure of the background zonal flow.

Extratropical Rossby waves have long been recognized as a potential source of energy for driving tropical circulations (e.g., Charney 1969; Mak 1969; Webster and Holton 1982; Zangvil and Yanai 1980). The propagation of such waves is

Corresponding author: Yuan-Ming Cheng, yuan-ming.cheng@noaa.gov

DOI: 10.1175/JCLI-D-22-0171.1

© 2022 American Meteorological Society. For information regarding reuse of this content and general copyright information, consult the AMS Copyright Policy (www.ametsoc.org/PUBSReuseLicenses).

Brought to you by NOAA Central Library | Unauthenticated | Downloaded 07/19/23 06:04 PM UTC

well understood on the basis of linear theory, which states that Rossby waves always travel westward relative to the mean flow in which they are embedded. As a consequence, eastward-moving Rossby waves at low latitudes must be advected by background westerlies, and can only propagate into low latitudes within regions of mean westerly flow (Charney 1969; Yang and Hoskins 1996). Thus many early studies focused on how the extratropics influence tropical circulations in regions of mean equatorial westerlies (e.g., K98; Tomas and Webster 1994). Upper-level westerlies are well developed over the east Pacific and Atlantic in the boreal cool seasons and these "westerly ducts" allow extratropical Rossby waves to intrude into the deep tropics. These transient eddies are crucial to the zonal momentum balance over the east Pacific (K98; Kiladis et al. 1994; Sakaeda and Roundy 2014).

Extratropical intrusions in a westerly duct have been well documented [Kiladis and Weickmann (1992), see sections 3 and 5a therein for more details; also see Knippertz (2007) for a review]. They are often associated with anticyclonic wave breaking near the exit region of the subtropical jet (Thorncroft et al. 1993; Shapiro et al. 2001). Consistent with their equatorward propagation, these transient circulations are positively tilted in a southwest–northeast manner in the Northern Hemisphere such that they transport westerly momentum poleward and disperse energy equatorward. Their positive potential vorticity anomalies lower the vertical stability and increase convective available potential energy. The associated quasigeostrophic (QG) forcing drives vertical motion in the subtropics and the ITCZ (K98; HSK20; Funatsu and Waugh 2008). The QG-forced cloudiness at the leading edge of the upper-level trough typically organizes into southwest–northeast-elongated "cloud plumes" that have been associated with the formation of atmospheric rivers (Bao et al. 2006; Ralph et al. 2011; Ryoo et al. 2013). Equatorial Rossby waves are also reported to form in the lower levels west of the convective region, which is likely a consequence of the excited convection (Kiladis and Wheeler 1995; Kiladis 1998; Matthews and Kiladis 2000). However, despite being coupled with convection in the tropics, the forced eastward-moving circulations retain much of their extratropical character (K98; HSK20).

Although linear theory predicts that an easterly basic state should prevent Rossby waves from moving into the lower latitudes due to critical lines, a handful of modeling and observational studies have in fact found equatorial waves remotely triggered by extratropical disturbances in regions of tropical easterlies (e.g., SK03; TK21; Kiladis et al. 2016; Yang and Hoskins 2013; Yang et al. 2018). In a dry barotropic framework, Zhang and Webster (1992) and Zhang (1993) demonstrated that the equatorial response to an imposed zonally moving mass source in the extratropics is strongly dependent on the frequency and translation speed of the forcing, as well as the direction of the background zonal wind. The largest Kelvin wave response was indeed found in equatorial easterlies rather than westerlies. Hoskins and Yang (2000), using a primitive equation model, investigated the equatorial response to imposed transient vorticity forcing in the midlatitudes under realistic basic states. They also found the largest amplitude of Kelvin waves in tropical mean easterlies for an eastward-moving forcing. Both Zhang (1993) and Hoskins and Yang (2000) concluded that this remote excitation is attributable to the close resonance between the Doppler-shifted frequency of forcing and the eigenfrequency of the equatorial modes. Using a global model with superparameterized physics, a recent study by TK21 showed how the extratropics can energetically excite and maintain Kelvin waves through momentum flux forcing associated with critical line effects. This energetic maintenance was seen to arise through an in-phase relationship between the momentum-flux forcing and Kelvin wave zonal wind anomalies, in accordance with the idea of wave resonance. In an observational study, SK03 showed that, despite the presence of mean easterlies, the initiation and activity of convectively coupled Kelvin waves appear to be associated with Rossby waves and their momentum flux from the Southern Hemisphere.

The goal of this study is to elucidate the mechanisms through which extratropical eddies excite convective disturbances in the tropics and clarify how these mechanisms depend on the meridional structures of the background zonal flow. Specifically, we use satellite observations and reanalysis data to compare and contrast the remote extratropical forcing of Kelvin waves documented in SK03, versus the local (intrusion-type) forcing of eastward-moving cloud plumes reported in K98 and HSK20. Given that the extratropical momentum flux appears to be relevant in both cases (SK03; TK21; K98; HSK20), primary attention is given to this quantity, which is analyzed in several different ways. The data and methods are described in section 2. Section 3 compares the climatological background states and wave activity associated with these two types of tropical disturbances. Section 4 investigates the remote pathway while section 5 examines the local mechanism. A summary and discussion of the results are provided in section 6.

2. Data and methods

a. Data

We used twice-daily satellite-derived outgoing longwave radiation (OLR; Liebmann and Smith 1996) from 1979 through 2019, along with the GPM IMERG (Global Precipitation Mission Integrated Multi-Satellite Retrievals) precipitation product (Huffman et al. 2020) available from 2001 through 2019. We also utilized the dynamical and thermodynamical fields from ERA5 (Hersbach et al. 2020) for the same period as OLR. Virtually identical results can be reproduced using ERA-Interim (Dee et al. 2011) and TRMM 3B42 (Huffman et al. 2007). Since the wave structures of interest have spatial scales in the synoptic to planetary range, all datasets were interpolated to a 2.5° grid for computation.

b. Empirical orthogonal function analysis

Empirical orthogonal function (EOF) analysis was used to extract tropical wave structures. EOFs were calculated through a covariance matrix approach using filtered OLR. We chose an eastward (excluding wave 0) 2–20-day filter that includes a broad spectrum of cloudiness signals, including Kelvin waves. Two separate EOF calculations were used for

Brought to you by NOAA Central Library | Unauthenticated | Downloaded 07/19/23 06:04 PM UTC

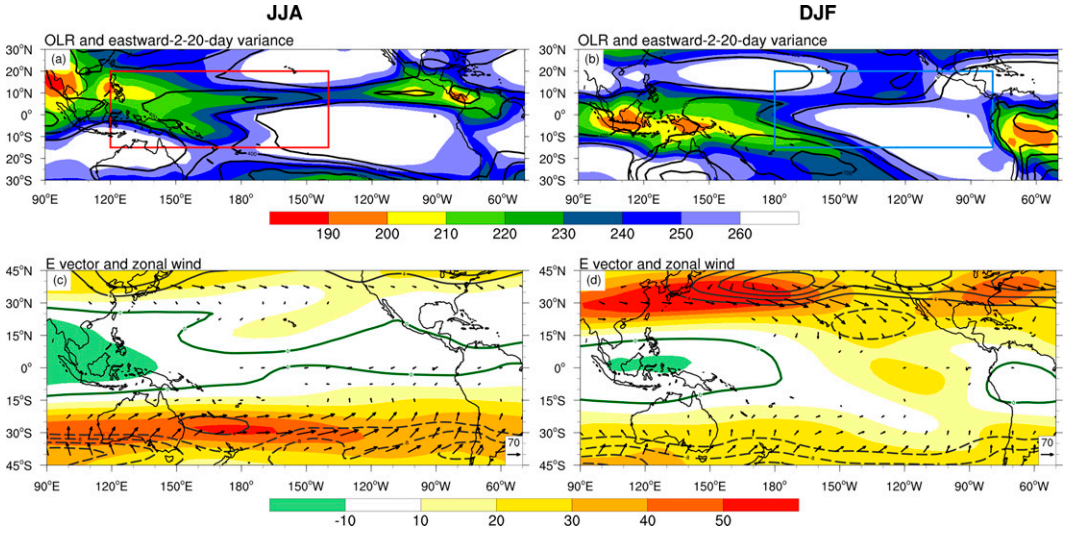

FIG. 1. (top) Climatological mean OLR (colors) and variance of eastward 2–20-day filtered OLR (contours) in (a) JJA and (b) DJF. (bottom) Climatological zonal wind (colors) and eastward 2–20-day filtered horizontal **E** vectors (vectors) and heat flux ($\overline{v'T'}$; contours) at 200 hPa for (c) JJA and (d) DJF. OLR is shaded in W m^{-2}. OLR variance is contoured every 150 W^2 m^{-4} starting from 250 W^2 m^{-4}. Zonal wind is shaded in m s^{-1} with zero zonal wind outlined by green contours. A reference for **E** vectors of 70 m^2 s^{-2} is shown in the bottom right corner. The heat flux is contoured every 4 K m s^{-1} with zero lines omitted. The red and blue boxes delineate the domains for Kelvin wave and cloud plume EOF.

the two types of tropical waves under consideration. The "Kelvin wave EOF" was calculated over the west-central Pacific (15°S–20°N, 120°E–140°W; see Fig. 1a) for June–August (JJA). For the cloud plumes, the "cloud plume EOF" was calculated over the east Pacific (15°S–20°N, 180°–80°W; Fig. 1b) for December–February (DJF). Circulations associated with the EOF patterns were obtained by projecting the raw reanalysis data of each grid point onto the time series of the principal component (PC), scaling to one standard deviation of the PC. A Student's t test was used to assess the statistical significance once the number of degrees of freedom was estimated through autocorrelation of both time series (Livezey and Chen 1983).

c. *Momentum flux forcing*

While equatorward-moving extratropical Rossby waves result in a poleward flux of westerly momentum and equatorward dispersion of energy, it is the convergence of the eddy momentum flux that acts as a driver of local changes in the momentum field (Randel and Held 1991; TK21). Therefore, we focus on the eddy momentum flux convergence/divergence and work with the eddy zonal momentum equation in pressure coordinates:

$$\frac{\partial u'}{\partial t} = \left(-u'\frac{\partial \overline{u}}{\partial x} - v'\frac{\partial \overline{u}}{\partial y} - \omega'\frac{\partial \overline{u}}{\partial p} - \overline{u}\frac{\partial u'}{\partial x} - \overline{v}\frac{\partial u'}{\partial y} - \overline{\omega}\frac{\partial u'}{\partial p} + fv' - \frac{\partial \phi'}{\partial x}\right) + F', \tag{1}$$

where u and v are zonal and meridional winds, ω is vertical pressure velocity, f is the Coriolis parameter, and ϕ is geopotential. The bars denote the seasonal average, and primes temporal anomalies about this average; F denotes the eddy momentum convergence, which is regarded here as a "forcing" and is given by

$$F = -\left(\frac{\partial u'u'}{\partial x} + \frac{\partial u'v'}{\partial y} + \frac{\partial u'\omega'}{\partial p}\right), \tag{2}$$

where $F > 0$ corresponds to westerly forcing and vice versa. On the right hand side of Eq. (1), all terms with the exception of F are linear source terms that collectively represent the effects of advection, the Coriolis force, and the zonal pressure gradient force.

Note that in the framework of wave–mean flow interactions, variables are partitioned into mean and eddy components. The forcing of the seasonal mean zonal wind is therefore given by the mean of the momentum flux forcing (i.e., $\overline{F}$; e.g., Hoskins et al. 1983; Randel and Held 1991). Because the focus here, however, is on the eddy driving of transient disturbances (i.e., Kelvin waves), we look to the eddy momentum equation [Eq. (1)] where the relevant forcing is F'. A limitation of this approach is that the two cases presented here involve Rossby waves encountering critical lines, as well the process of Rossby wave breaking, so the linear framework may not fully account for the full range of nonlinear interactions. Nonetheless, our analysis will highlight the significance of the nonlinear processes in forcing tropical circulations.

The corresponding zonal eddy kinetic energy (EKE) equation is derived by multiplying Eq. (1) by u' to obtain

Brought to you by NOAA Central Library | Unauthenticated | Downloaded 07/19/23 06:04 PM UTC

$$\frac{1}{2}\frac{\partial u'^2}{\partial t} = u'\left(-u'\frac{\partial \overline{u}}{\partial x} - v'\frac{\partial \overline{u}}{\partial y} - \omega'\frac{\partial \overline{u}}{\partial p} - \overline{u}\frac{\partial u'}{\partial x} - \overline{v}\frac{\partial u'}{\partial y} - \overline{\omega}\frac{\partial u'}{\partial p} + fv' - \frac{\partial \phi'}{\partial x}\right) + u'F'. \quad (3)$$

This equation states that the covariance between u' and terms on the right-hand side acts as a source of EKE. An in-phase relationship between u' and its forcing is expected for any sort of resonantly forced mode of oscillation.

d. *E* vectors

The propagation of Rossby wave energy can be described by **E** vectors (Hoskins et al. 1983), defined as

$$\mathbf{E} = \left(\overline{v'^2 - u'^2},\ -\overline{u'v'},\ f_0\frac{\overline{v'\theta'}}{\Theta_p}\right), \quad (4)$$

where f_0 is the Coriolis parameter and $\Theta_p = \partial\overline{\theta}/\partial p$ represents the mean vertical static stability. The primes denote eastward 2–20-day filtering and the bars represent an average over the season. Under the QG approximation, the **E** vectors approximately point in the direction of the Rossby wave group velocity and energy propagation. The **E** vector convergence corresponds to the eddy forcing to weaken westerly mean flow. While the QG assumptions involved to derive **E** vectors are not completely valid in regions of wave breaking such as over the east Pacific, they nonetheless provide a qualitative guidance on Rossby energy propagation.

e. Dispersion relationship of barotropic Rossby waves

The dispersion relationship for linear barotropic Rossby waves can be described as (e.g., Hoskins and Karoly 1981)

$$\omega = \overline{u}_M k - \frac{\beta_M k}{k^2 + l^2}, \quad (5)$$

where ω is frequency, $\overline{u}$ is the zonal mean wind, β is the meridional gradient of absolute vorticity, and k and l are the zonal and meridional wavenumbers, respectively. The subscript M denotes a Mercator projection on a sphere, which is a well-accepted approximation for simplifying the analysis (e.g., TK21; Hoskins and Karoly 1981; Karoly 1983). Equation (5) was used to calculate dispersion relationship in Figs. 2c and 2d for various values of l, where u_M and β_M were estimated using the climatological zonal wind at 300 hPa averaged across the latitude band and longitude range of the domain.

f. Spectral and cross-spectrum analysis

Spectral analysis was used to decompose the zonally propagating disturbances into wavenumber and frequency space (Wheeler and Kiladis 1999). Cross-spectrum analysis was used to determine the statistical relationship between two different variables, as a function of zonal wavenumber and frequency (Hendon and Wheeler 2008). The analysis was performed for JJA and DJF and over the two sectors of interest: west-central Pacific (120°E–140°W) and east Pacific (180°–80°W) using a zonal windowing approach (Dias and Kiladis 2014). Note that the signal in the low wavenumber cannot be explicitly resolved due to the zonal windowing and needs to be interpreted with caution. Two-dimensional Fourier transforms were calculated for each season, after the seasonal cycle (defined as the first three harmonics of the annual cycle) was removed. A 10% tapering was used at the ends of the time series and zonal boundaries. The real part of the cross-spectrum is the cospectrum, which shows the positive (in phase) and negative (out of phase) contributions to the total covariance.

g. Latitude–phase speed diagram

To characterize the transient eddy forcing, regional momentum flux spectra were calculated as a function of latitude and zonal phase speed, following the approach of Randel and Held (1991). Applying the chain rule to the definition of F, the forcing was first calculated in flux form via cross-spectral analysis, followed by interpolation from frequency to zonal phase speed using a method designed to ensure conservation of the spectral covariance [see Randel and Held (1991) for details].

h. Meridional projection

Previous studies have used various decomposition methods to study equatorial waves (Knippertz et al. 2022). One common technique is to spectrally decompose the data in terms of zonal wavenumber and frequency, as in Wheeler and Kiladis (1999). However, because the solutions to the linear shallow water equations on an equatorial β plane have parabolic cylinder functions as their meridional basis, several studies have further decomposed structures in the meridional direction (e.g., Gill 1980; Yang et al. 2003; Gehne and Kleeman 2012; Haertel 2021; TK21).

Following TK21, we adopted a meridional projection using the first parabolic cylindrical function. This structure function is a Gaussian centered at the equator that describes the meridional structure of theoretical Kelvin waves. Meridionally projected zonal wind (u_p) and momentum flux forcing (F_p) are defined as

$$u_p(t,\lambda) = \frac{1}{\pi}\int_{-\pi/2}^{\pi/2} u(t,\lambda,\phi)\exp\left[-\left(\frac{\phi}{2\phi_0}\right)^2\right]d\phi, \quad (6)$$

$$F_p(t,\lambda) = \frac{1}{\pi}\int_{-\pi/2}^{\pi/2} F(t,\lambda,\phi)\exp\left[-\left(\frac{\phi}{2\phi_0}\right)^2\right]d\phi, \quad (7)$$

where u and F have dimensions of time, longitude, and latitude. The trapping scale ϕ_0 is taken as 9° on the basis of a multivariate EOF analysis (see the appendix). Previous studies have reported a wide range of ϕ_0 from 5° to 14° (e.g., Takayabu 1994; Kiladis and Wheeler 1995; Wheeler and Kiladis 1999; Yang et al. 2003; Gehne and Kleeman 2012) using various methods and variables for different equatorial waves. Here the multivariate EOF analysis using variables with strong Kelvin wave signal—OLR and zonal divergent

Brought to you by NOAA Central Library | Unauthenticated | Downloaded 07/19/23 06:04 PM UTC

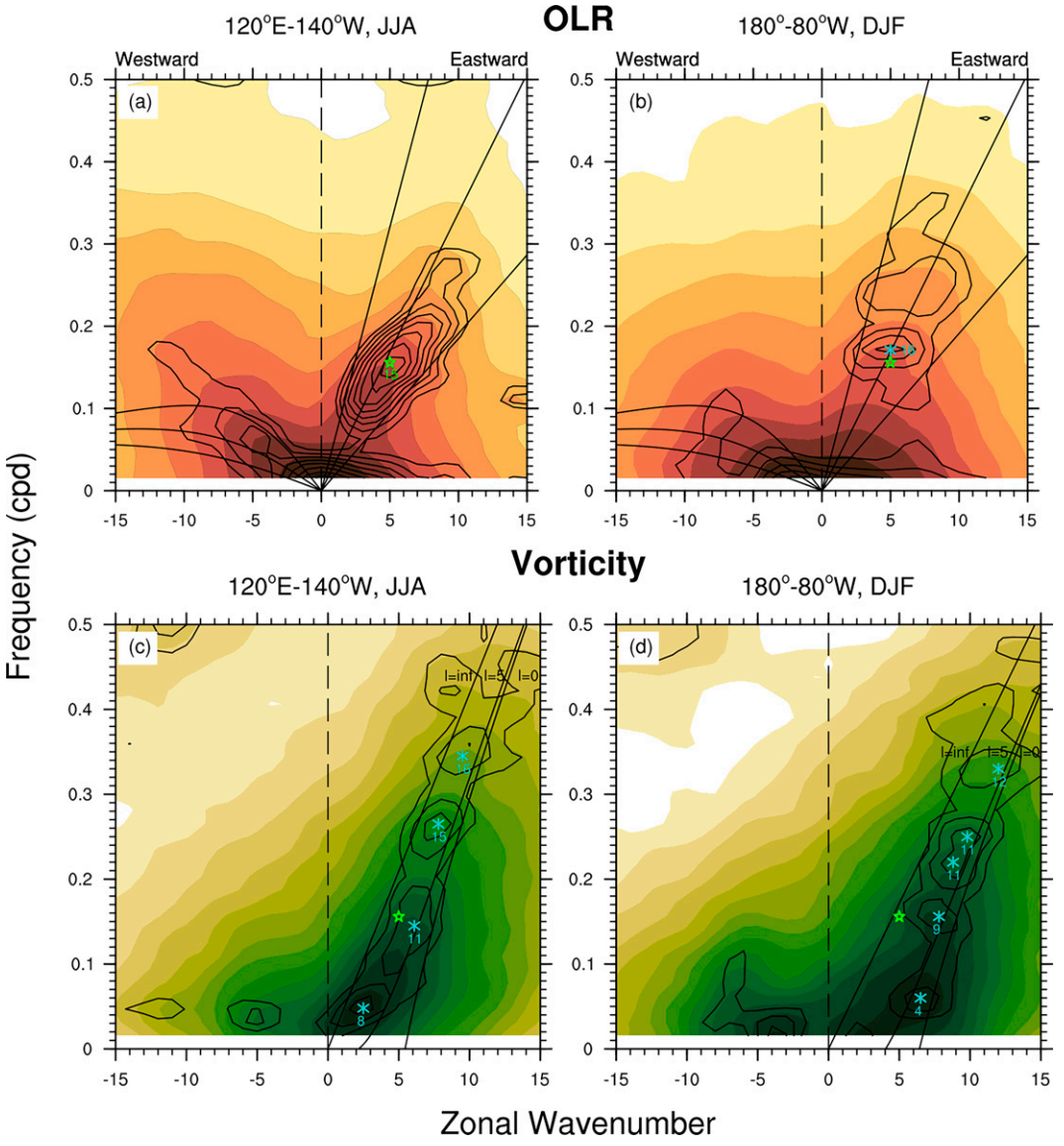

FIG. 2. Wavenumber–frequency power spectrum over (a),(c) 120°E–140°W in JJA and (b),(d) 180°–80°W in DJF. (top) The symmetric component of OLR power summed over 15°S–15°N. (bottom) Vorticity spectra summed over 20°–15°S in (c) and 15°–20°N in (d). Contours denote the ratio between the raw power and a smoothed background following Wheeler and Kiladis (1999). Color shadings are the raw power for reference. In the top panel, dispersion curves for Kelvin and equatorial Rossby waves are overlaid for equivalent depth of 8, 25, and 90 m. In the bottom panel, dispersion curves of Rossby waves are drawn for $l = 0$, 5, and infinity, calculated with climatological mean zonal wind at 300 hPa in each domain using Eq. (5). Green stars repeated in each panel mark the peak wavenumber and frequency of Kelvin waves (wavenumber 5 and period of 6.5 days) and the corresponding phase speed ($c = \omega/k$) in (a) while cyan asterisks indicate prominent spectral peaks and their phase speeds.

wind—is able to extract the dominant meridional structure, which is suitable for determining ϕ_0 for Kelvin waves in this region and season. The results are qualitatively similar with a trapping scale of 6°–10°.

Unlike TK21, the projection here does not involve any distinction between tropical versus extratropical components, since the amplitude and forcing of the Kelvin-mode eigenstructure depends on the full (tropical-to-extratropical) projection. Results delineating the extratropical versus tropical components in the case of Kelvin waves were found to be similar to those obtained in TK21 (not shown).

Using the above basis function projection makes estimating the equatorial mode response to the extratropical forcing mathematically consistent with the linearized shallow

Brought to you by NOAA Central Library | Unauthenticated | Downloaded 07/19/23 06:04 PM UTC

water equations on an equatorial β plane. However, the projection is only a meridional decomposition and other waves can also contribute to the same Gaussian distribution. Further information such as wavenumber, frequency, and wave structure is needed to determine whether a Kelvin wave disturbance is actually present.

3. Climatological basic states and wave characteristics

This section describes the climatological background states and underlying wave characteristics relevant to the two extratropically forced disturbances in the tropics: Kelvin waves in prevailing easterlies across the Pacific during JJA and eastward-moving tropical cloud plumes over the east Pacific within the westerly duct during DJF. The relationship between the background wind and resonance will also be investigated as an extratropical forcing pathway.

a. Climatological basic states

Figure 1 shows the climatological OLR from satellites and dynamical fields from ERA5 in JJA and DJF, 1979–2019. The climatological OLR in colors indicates that the strongest mean convection occurs during northern summer across the Asian and North American monsoon regions over land, while the weakest convection occurs over the central-east Pacific (Fig. 1a). Synoptic variability of convection is depicted in contours as the variance of eastward-propagating, 2–20-day filtered OLR, to represent the broad spectrum of eastward-moving disturbances over the equatorial Pacific (see also Fig. 2). High convective activity is seen across the Pacific with maximum variance occurring just east of the date line along the axis of the ITCZ between 5° and 10°N. This region also exhibits the highest Kelvin wave activity in this season (e.g., SK03; Roundy and Frank 2004; Huang and Huang 2011). While Kelvin waves are modulated by climatological mean conditions along the ITCZ, such as sea surface temperature and low-level moisture, the fact that the Kelvin wave activity peaks in a region where mean convection activity is relatively weak suggests that other factors, such as extratropical forcing, are more important for determining their activity (SK03).

Collocated with the convectively active regions are mean upper-level equatorial easterlies, whose boundaries approximately outline the mean ITCZ (green shading and contours in Fig. 1c). The extratropics is dominated by a strong subtropical jet centered at 30°S, with the jet core extending from the Indian Ocean to the east Pacific. High Rossby wave activity stretches along the jet and extends into the subtropics (not shown; see Fig. 1 of SK03). The **E** vectors describe the propagation of Rossby wave energy under the QG approximation (see section 2d). Figure 1c shows the horizontal component of the **E** vectors in vectors with the vertical component approximated by heat flux ($\overline{v'T'}$) in contours. On the equatorward side of the subtropical jet, the Rossby waves disperse their energy northeastward over Australia toward the tropics, as implied by the northeast-pointing vectors. The positive heat flux around 25°S and 105°E–180° indicates a downward Rossby wave propagation, but the associated forcing is weak in comparison to that of the horizontal component of **E** vectors (not shown). The convergence of **E** vectors between 15° and 20°S, as implied by decreasing magnitude with latitude, indicates that the net effect of the eddies is to create wave drag and slow down the mean subtropical westerlies, while strengthening the adjacent easterlies. In addition to this net effect on the mean flow, however, results in section 3 will show how such eddy forcing also acts to excite transient Kelvin wave disturbances.

The large-scale environment observed during northern winter (Figs. 1b,d) over the east Pacific is quite different from that over the broader Pacific during northern summer. A region of seasonal mean high clouds (in colors) extends poleward into the subtropics over the east Pacific. The high clouds are collocated with high variance in eastward-moving OLR signals in contours. Despite the meridionally broad region of high clouds, the ITCZ, where deep convection occurs, is confined to a narrow band between the equator and roughly 10°N (see Fig. 3 of HSK20), indicative of the fact that the locally low mean OLR over the east Pacific and high OLR variance primarily represent upper-level clouds with weak precipitation.

The low-latitude westerlies over the east Pacific provide a pathway for extratropical Rossby waves to propagate directly into the equatorial region and potentially through to the Southern Hemisphere (Kiladis and Weickmann 1992; Tomas and Webster 1994; Matthews and Kiladis 2000). Following the waveguide, baroclinic waves generated within the storm track propagate along the Asian–Pacific jet until they reach the exit region, where some break anticyclonically, resulting in dispersion into the lower latitudes [see Fig. 4 of Matthews and Kiladis (1999a)]. The southeast-pointing **E** vectors over the subtropical Pacific reflect this equatorward propagation of energy. The countergradient negative heat flux is indicative of downward energy propagation (contours in Fig. 1d), although the forcing due to the divergence of this flux is relatively small as in the JJA case (not shown). The convergence of horizontal **E** vectors in the subtropics implies a deceleration of the mean westerlies by the eddies.

b. Wave characteristics

To compare the spectral properties of disturbances in the tropics versus extratropics in both seasons, the wavenumber–frequency spectrum of OLR and vorticity is shown in Fig. 2. In JJA, the former is calculated between 15°S and 15°N while the latter between 15° and 20°S, in the longitude range of 120°E–140°W. For the vorticity spectrum, the dispersion relationship for linear barotropic Rossby waves is calculated and overlain as described in section 2e.

The familiar signals of Kelvin waves are readily apparent in the OLR spectrum of Fig. 2a, with the strongest signals occurring at eastward-moving zonal wavenumbers 5 and periods of the range 6–8 days, corresponding to propagation speeds of around 15 m s^{-1}. The vorticity spectrum (Fig. 2c) shows that rotational eddies in the subtropics are predominantly eastward-propagating as well, with dispersion broadly matching the theoretical curves for linear barotropic Rossby waves.

Brought to you by NOAA Central Library | Unauthenticated | Downloaded 07/19/23 06:04 PM UTC

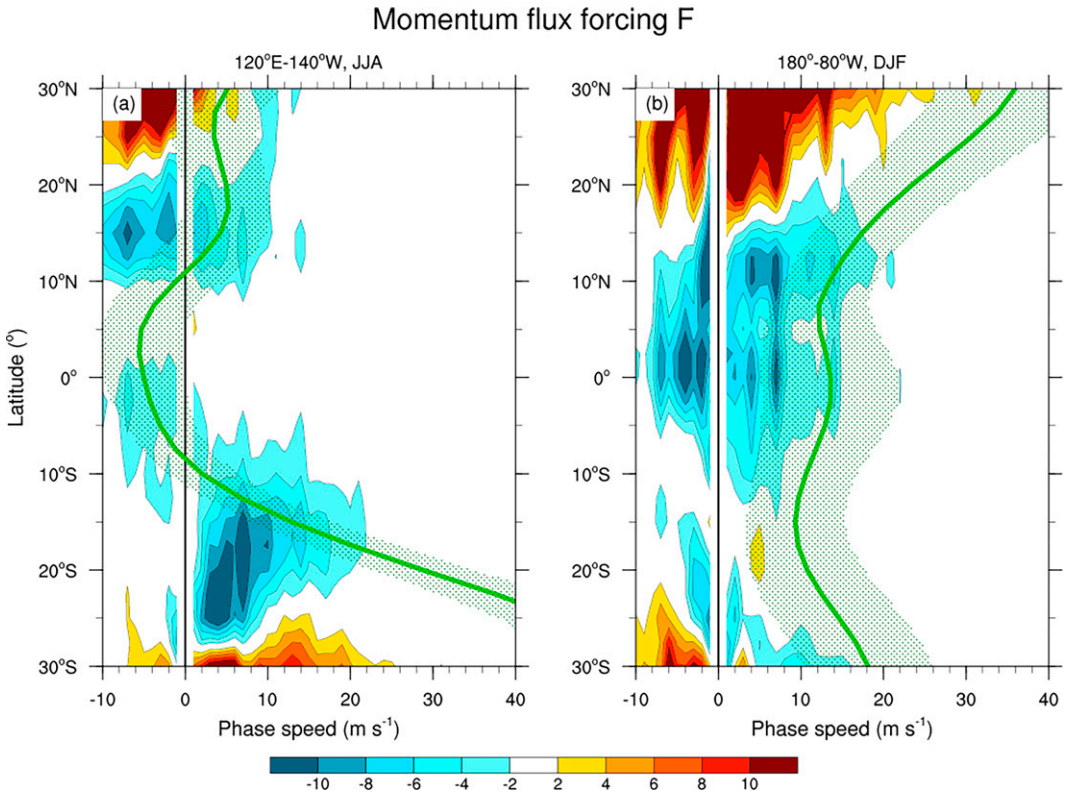

FIG. 3. Latitude–phase speed diagram of eddy momentum flux convergence $F = -(\partial u'u'/\partial x + \partial u'v'/\partial y + \partial u'\omega'/\partial p)$ over (a) 120°E–140°W in JJA and (b) 180°–80°W in DJF. The momentum flux forcing (10^{-8} m s^{-2}) is averaged across wavenumbers 1–10. The green line denotes the seasonal mean zonal wind, and the stippling denotes ±1 daily standard deviation of each sector.

Peak signals occur between zonal wavenumber 5–10 at periods less than 10 days, and shift to lower zonal wavenumbers at lower frequencies. The synoptic-scale signals represent the imprint of equatorward propagating extratropical disturbances (Randel and Held 1991), while the dominance of power at lower wavenumbers can be partly attributed to the fact that long waves are more effective at penetrating into the tropics due to their slower phase speeds (Straus and Lindzen 2000). Substantial power overlaps those of the Kelvin wave signals in the OLR spectrum. This overlap implies that extratropical disturbances can potentially excite Kelvin wave disturbances, provided the extratropical forcing projects onto the meridional Kelvin-mode eigenstructure (Zhang 1993; Hoskins and Yang 2000).

When equatorward-propagating eddies approach their critical line, the momentum flux convergence and divergence acts as a transient forcing of the zonal wind (Randel and Held 1991). Figure 3a characterizes the latitudinal distribution of momentum flux forcing (F) as a function of zonal phase speed. We average across zonal wavenumbers 1–10 to emphasize the forcing relevant to planetary and synoptic-scale disturbances in the tropics (cf. Figs. 2a,c). Linear theory predicts that the peak power should align with the critical line, but the maximum forcing is actually shifted about 5°–10° poleward of the critical line, similar to the findings of Randel and Held (1991). Because the speed of the background zonal wind generally decreases toward the equator, faster eddies tend to encounter their critical lines at higher latitudes. In the Southern Hemisphere, the forcing peaks at between 5 and 10 m s^{-1}, but spans a wide range of phase speeds, including the average phase speed of Kelvin waves at 15–20 m s^{-1}, in agreement with the vorticity spectrum in Fig. 2c. This contrasts with the picture in Fig. 3b for the east Pacific, as we discuss next.

Figures 2b and 2d display the OLR and vorticity spectra for the east Pacific in DJF in the longitudes of 180°–80°W. The OLR spectrum shows a relatively broad lobe of enhanced power at eastward-moving zonal wavenumbers in the synoptic range, with signals peaking at overall higher

TABLE 1. Estimated steering flow ($\overline{u}_s$) and phase speed of the forcing for resonance c_f in JJA and DJF. The $\overline{u}_s$ is estimated by averaging 5°N–5°S zonal wind across 120°E–140°W for JJA and 180°–80°W for DJF at 300 hPa. The intrinsic phase speed of Kelvin waves (c_K) is estimated to be 20.8 m s^{-1} for both seasons. See text for more details.

	$\overline{u}_s$	c_f
JJA	−5.8	20.8
DJF	6.8	27.6

Brought to you by NOAA Central Library | Unauthenticated | Downloaded 07/19/23 06:04 PM UTC

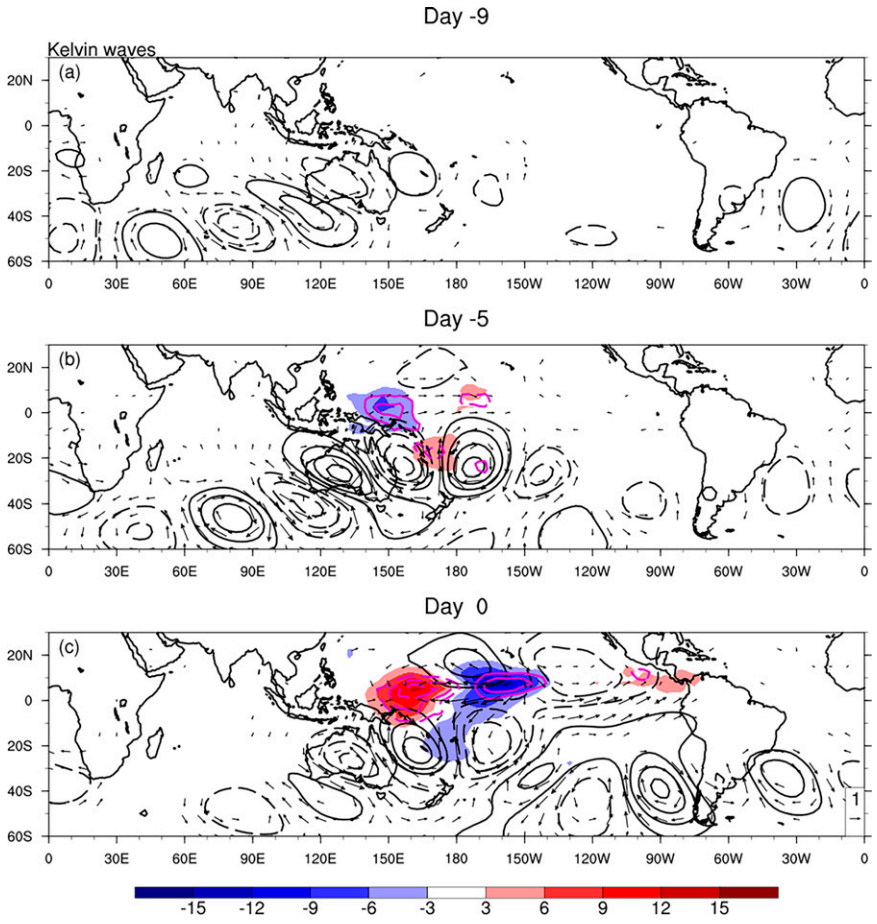

FIG. 4. Anomalous OLR (colors; W m^{-2}), 200-hPa streamfunction (black contours), wind vectors (vectors), and GPM IMERG precipitation (magenta contours) regressed onto PC1 of the Kelvin wave EOF during JJA from day −9 through 0. Streamfunction is contoured every 6×10^5 m^2 s^{-1} in black with zero lines omitted. GPM IMERG precipitation is contoured every 0.05 mm h^{-1} in magenta with zero lines omitted. A reference wind vector of 1 m s^{-1} is shown in the bottom-right corner. Only fields that are statistically significant at the 95% interval are shown.

frequencies and zonal wavenumbers than in the corresponding JJA case (Fig. 2a). While the OLR signals appear to align with the Kelvin wave dispersion line, their associated dynamical structures are found be extratropical in nature (as shown later in Fig. 14; see also HSK20). The subtropical vorticity spectrum is dominated once again by eastward-moving signals with dispersion matching that of linear Rossby waves. The signals in this case, however, are shifted toward slightly higher zonal wavenumbers and somewhat slower phase speeds, presumably due to the weaker background zonal flow speed in their corresponding sectors (10 m s^{-1} during DJF vs 17 m s^{-1} during JJA).

Figure 3b shows the momentum flux convergence over the east Pacific. As in the JJA case, the shape of the forcing approximately follows the zonal mean wind, consistent with eddies encountering their critical lines and depositing their zonal momentum flux. However, the westerly duct in this case allows the eddy forcing to extend into the equatorial region for phase speeds less than roughly 10 m s^{-1}.

c. *Resonance and the background zonal wind*

Although Kelvin waves are often seen over the east Pacific during El Niño winters, this occurs under the anomalous conditions of higher than normal sea surface temperatures over that region, when upper tropospheric easterlies are dominant and the basic state is more like that over the warm pool (Wang et al. 2013; Yang and Hoskins 2013; Das and Pan 2016). Otherwise, under normal or La Niña conditions, tropical cloud plumes are the overwhelmingly dominant disturbances (section 5). This observation may come as a surprise, given that the spectrum of extratropical eddy forcing in the DJF case is not all that different from what is apparent in the JJA case, where Kelvin waves are the norm (cf. Figs. 3a,b). While several different factors could be responsible for the dearth of Kelvin waves over the east Pacific during DJF (including the presence of westerly mean vertical shear in the ITCZ; Guo et al. 2014; Wang and Chen 2016), here it is hypothesized that a key reason is due to the properties of the background state being generally unsuitable for wave resonance between the tropics and extratropics.

Brought to you by NOAA Central Library | Unauthenticated | Downloaded 07/19/23 06:04 PM UTC

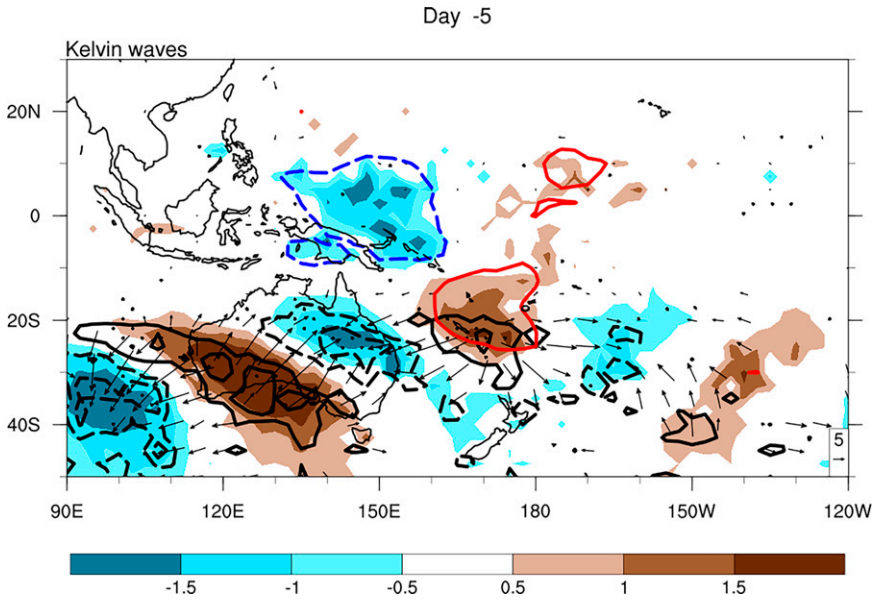

FIG. 5. Anomalous 350-hPa ω (colors; 10^{-2} Pa s^{-1}), **Q** vectors (vectors), and their divergence (black contours) regressed onto PC1 of the Kelvin wave EOF during JJA for day −5. The **Q** vector divergence is contoured every 1.5×10^{-17} Pa^{-1} s^{-3} with negative values (convergence) dashed and zero lines omitted. A reference **Q** vector of 5×10^{-12} m Pa^{-1} s^{-3} is shown in the bottom-right corner. For reference, the anomalous OLR at ±3 K is also overlaid in blue and red contours. Fields plotted are statistically significant at the 95% interval except for **Q** vector divergence, in which stippling shows significance at the 90% interval to highlight a coherent pattern as the calculation involves the product of vorticity and temperature gradients. Both fields are noisy by nature.

As laid out in the work of Zhang (1993) and Hoskins and Yang (2000), wave resonance requires the frequency of the extratropical eddy forcing to be close to that of the Doppler-shifted Kelvin wave. Assuming that the zonal scales of the wave and forcing remain roughly invariant during their life cycle, the phase speed of the forcing must then be close to that of the Doppler-shifted Kelvin wave speed, that is,

$$c_f \cong \overline{u}_s + c_K, \tag{8}$$

where c_f is the phase speed of the forcing, $\overline{u}_s$ is the steering flow, and c_K is the intrinsic Kelvin wave speed. To estimate the intrinsic phase speed of Kelvin waves, an assumption is needed concerning the vertical level of the steering flow. Here, we appeal to observations and simulations, both of which point to this level as residing in the tropical upper troposphere at around 300 hPa (Dias and Kiladis 2014; Tulich and Kiladis 2021). The implied value of $\overline{u}_s$ in the JJA case is thus estimated to be around −6 m s^{-1} (average across 5°N–5°S, 120°E–140°W). Based on the peak Kelvin wave signal in the OLR spectra of roughly 15 m s^{-1} (Fig. 2a), the intrinsic phase speed of Kelvin waves c_K is then estimated to be around 21 m s^{-1} (Table 1). This implied value of c_K is close to that inferred by TK21 on the basis of their idealized simulations of Kelvin waves under different imposed background flow regimes (see their Fig. 16).

The steering flow in the DJF case is estimated to be around 7 m s^{-1}. The required value of c_f is thus even faster than during JJA at roughly 28 m s^{-1}. The fact that eddy forcing at this eastward-moving phase speed is generally negligible in the subtropics over the east Pacific during DJF (as evidenced in Fig. 3b) is presumably the main reason why relatively slow-moving tropical cloud plumes, as opposed to faster Kelvin waves, are observed to be the dominant response to such forcing in this case. More concrete evidence to support this idea is presented in the next two sections, which deals with the forcing pathways of Kelvin waves and eastward-moving tropical cloud plumes, respectively.

4. Remote pathway: Kelvin waves

This section investigates how the extratropics excite Kelvin waves. We first look at QG forcing and then momentum flux forcing in regression analysis. We then turn to the spectral space to highlight that momentum flux forcing indeed can resonate with Kelvin waves with similar wavenumber and frequency. Last we conduct a momentum budget to highlight the contribution from the momentum flux forcing.

a. Extratropical Rossby waves

Figure 4 displays the first EOF of eastward 2–20-day filtered OLR (colors) in JJA, and the associated circulation (vectors and black contours), and precipitation (magenta lines). While the higher EOFs can also include signals from smaller-scale Kelvin waves (Roundy 2015), we focus on the first two EOFs that explain the most variance. The first two

Brought to you by NOAA Central Library | Unauthenticated | Downloaded 07/19/23 06:04 PM UTC

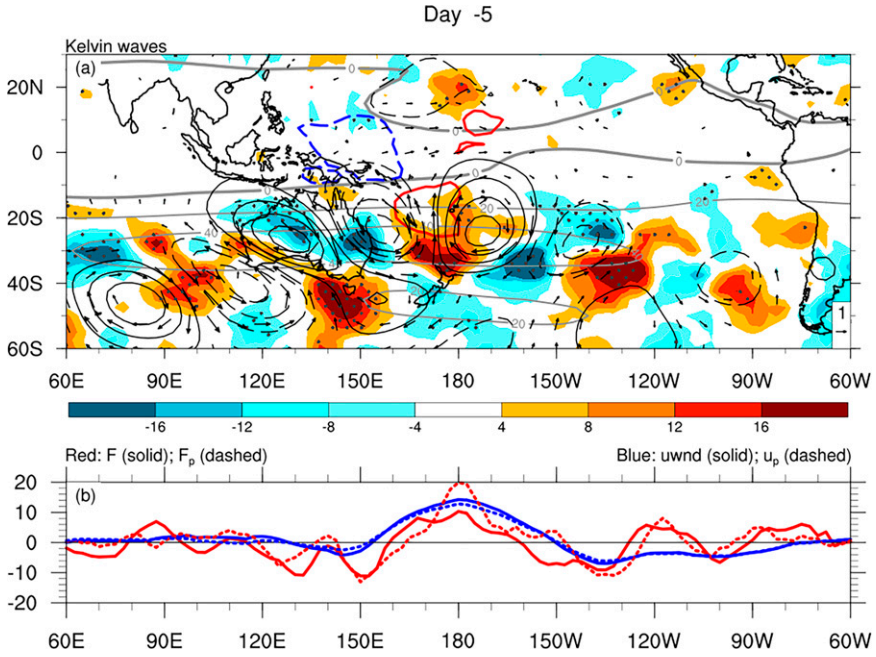

FIG. 6. (a) Map of anomalous 200-hPa momentum flux forcing (F; colors), wind (vectors), and streamfunction (black contours) and (b) line graph of 200-hPa F (red), zonal wind (u; blue), and meridionally projected momentum flux forcing (F_p; red dashed) and zonal wind (u_p; blue dashed) regressed onto PC1 of the Kelvin wave EOF during JJA for day −5. In (a), F is shaded in 10^{-6} m^2 s^{-3}. Streamfunction is contoured every 6×10^5 m^2 s^{-1} in black with zero lines omitted. Fields shown are statistically significant at the 95% interval except for momentum flux forcing, in which stippling shows statistical significance at the 90% interval to highlight coherent patterns as the field is intrinsically noisy due to the gradient of eddy covariance. For reference, the mean zonal wind of JJA is plotted in gray contours at 20 m s^{-1} interval. The anomalous OLR at ±3 K is also overlaid in blue and red lines. In (b) u and u_p are scaled by a factor of 20 and 120 while F and F_p by 10^6 and 3×10^7 for plotting purposes.

EOFs explain 5.7% and 5.5% variance of the band, and form a quadrature pair, with their PCs correlated at 0.78 for a 2-day lag, implying an eastward-propagating disturbance with a period of around 8 days. Figure 4 closely resembles Fig. 2 of SK03, which was calculated using a one-point regression against more restrictive Kelvin-wave-filtered OLR. This close resemblance confirms that our less restrictive EOF analysis is able to isolate the same Kelvin waves as studied in SK03.

Figure 4 shows that a globally circumnavigating wave train, stretching from South America to east of Australia in the extratropics, precedes the peak convection of Kelvin waves by 9 days. The positively tilted eddies around Australia transport westerly momentum poleward and disperse energy equatorward, as seen by connecting the circulation centers. This equatorward dispersion is consistent with the mean Rossby wave behavior in the region (**E** vectors in Fig. 1). The Kelvin wave's convection and circulation anomalies are well established by day −5 (Fig. 4b) and reach peak intensity over the central Pacific on day 0 (Fig. 4c). As pointed out in SK03, the fact that the extratropical wave packet appears prior to and upstream (i.e., to the west) of the Kelvin wave strongly suggests that the former excites the latter. However, the precise mechanism of this initiation has yet to be delineated.

QG forcing is arguably the most straightforward pathway in which extratropical Rossby waves can affect tropical cloud and precipitation processes (e.g., Funatsu and Waugh 2008; Fischer et al. 2017). The temperature and vorticity advection of Rossby waves leads to the dynamical forcing of vertical motion to maintain thermal wind balance. Such forcing can be effectively diagnosed using **Q** vectors (Hoskins et al. 1978). While **Q** vector diagnostics are only meaningful in regions where QG balance is valid, Kiladis et al. (2006) demonstrated their qualitative utility in the tropics for off-equatorial Rossby-type disturbances. Following their formulation, **Q** vectors are calculated by replacing the total wind with the rotational wind. Figure 5 shows the anomalous **Q** vectors (vectors), their convergence (contours) as well as vertical motion at 350 hPa (colors), close to where upward motion peaks in the subtropics. Convergence of **Q** vectors corresponds to forcing of upward motion and vice versa. In the tropics, upward motion matches high cloud tops, indicative of deep convection. Poleward of 20°S, there is a clear correspondence between the dynamical QG forcing and the vertical motion. The upward motion centered at 150°E over northeastern Australia, for example, matches well with **Q** vector convergence. This region is in the northwesterly flow of a trough (Fig. 4b)

Brought to you by NOAA Central Library | Unauthenticated | Downloaded 07/19/23 06:04 PM UTC

where there is strong vorticity and temperature advection (not shown). The QG forcing, however, stays removed from the equatorial convective envelope of the Kelvin wave, indicating that such extratropical forcing has a minimal direct impact on this type of tropical disturbance. This result is perhaps not surprising, since the background easterlies prevent extratropical Rossby waves from propagating into the tropics.

b. *Momentum flux forcing*

Previous studies have looked at momentum flux to infer energy transport into the tropics by Rossby waves (e.g., K98; SK03; HSK20; Yang and Hoskins 2013; Yang et al. 2018; **E** vectors in Fig. 1). Zangvil and Yanai (1980) attempted to use momentum flux and the mean zonal wind profile to deduce the extratropical contribution to equatorial EKE through barotropic conversions, but found no clear signal for Kelvin waves due to equatorial easterlies and critical line absorption. Here we hypothesize that it is the momentum flux convergence/divergence F due to critical line effects that acts as forcing, which projects onto the meridional structure of Kelvin waves and drives their circulations. Figure 6 shows the spatial pattern of the anomalous momentum flux forcing (colors) associated with the Kelvin wave at day −5. When the transient eddies move equatorward near Australia, they encounter critical lines. Linear theory breaks down near the critical line and a thorough nonlinear analysis is required to understand the wave behavior. Here we apply a simple dispersion relationship to conceptually understand how waves may behave when approaching the critical line. Since zonal phase speed is given as $c = \omega/k$, which is $\overline{u}_M - [\beta_M/(k^2 + l^2)]$, solving Eq. (5) for l^2 gives

$$l^2 = \frac{\beta}{\overline{u}_M - c} - k^2. \tag{9}$$

As a wave approaches its critical line in the subtropics, $\overline{u}_M - c$ gets increasingly small and l^2 increasingly large. The meridional wavelength shrinks rapidly, and the waves are absorbed by the mean flow, depositing their momentum as a forcing to drive transient circulations. Consistent with this narrative, Fig. 6 shows that the waves become highly tilted and their meridional scale shrinks. These circulations are accompanied by strong momentum flux forcing at subtropical latitudes. This extratropical forcing and circulation (Fig. 4) appear days before the OLR signal.

Following TK21, we adopt the meridional projection approach (section 2h) to estimate the remote eddy momentum flux forcing of Kelvin-mode circulations. The projection conveys how strongly the forcing projects onto the Kelvin mode's meridional eigenstructure. Because this structure decays exponentially with distance from the equator, the efficacy of the projection will have a strong dependence on the meridional distribution of F, arguing against the use of simple meridional averaging. To illustrate, Fig. 6b compares the 30°–15°S average (solid) and meridionally projected (dashed) zonal wind and momentum flux forcing. Overall the two methods show similar patterns for the zonal wind but more discrepancy for the momentum flux forcing, due to the projection's greater emphasis on forcing perturbations at the lower latitudes.

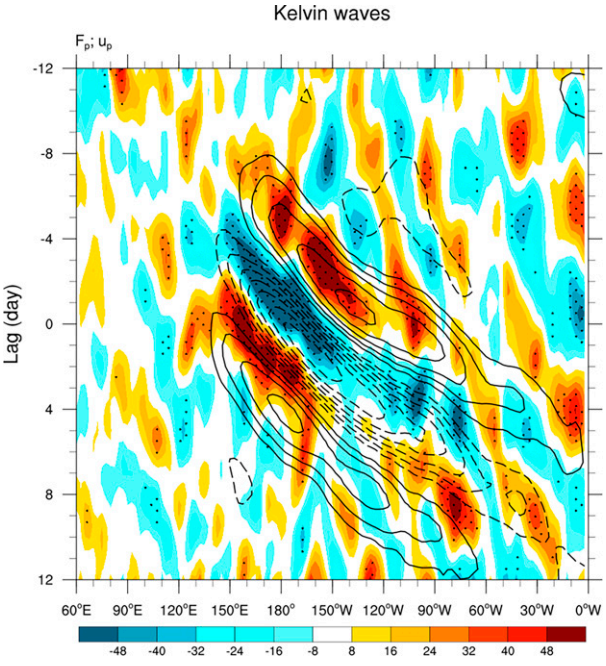

FIG. 7. Hovmöller diagram of anomalous meridionally projected zonal wind (u_p; contours) and momentum flux forcing (F_p; colors) at 200 hPa regressed onto PC1 of the Kelvin wave EOF during JJA. Zonal wind is contoured every 3×10^{-2} m s^{-1} with zero lines omitted. Negative values are dashed. Momentum flux forcing has a unit of 10^{-8} m^{-2} s^{-3}. Only statistically significant u_p at the 95% interval is plotted. Stippling shows F_p statistically significant at the 90% interval.

Figure 7 shows the Hovmöller of meridionally projected zonal wind u_p (contours) and momentum flux forcing F_p (colors). The two fields evolve coherently with one another across the western and central Pacific, where Rossby-type eddies display the strongest equatorward propagation and energy transport (Figs. 4 and 6). Figure 7 shows that F_p comprises both large- and small-scale signals, with the latter displaying intermittent strengthening and weakening. The larger-scale signals move eastward at roughly 16 m s^{-1}, similar to the Kelvin wave signals in u_p. This close correspondence suggests the relevant extratropical forcing for Kelvin waves has relatively large zonal scales, which correspond to small meridional wavelengths (or large values l) as implied by the vorticity spectrum in Fig. 2c. The momentum flux forcing can be traced back around 90°E on day −12 before the development of u_p (Fig. 7). Once the Kelvin wave is established on day −8, F_p becomes nearly in phase with u_p. This in-phase relationship suggests the momentum flux forcing acts to excite and maintain Kelvin wave zonal wind anomalies through generation of EKE [Eq. (3)], as expected for a resonantly forced mode of oscillation. This apparent resonance, however, falls apart as signals in u_p become weaker and more diffuse east of 150°W over the Western Hemisphere, where F_p propagation also becomes more erratic,

Brought to you by NOAA Central Library | Unauthenticated | Downloaded 07/19/23 06:04 PM UTC

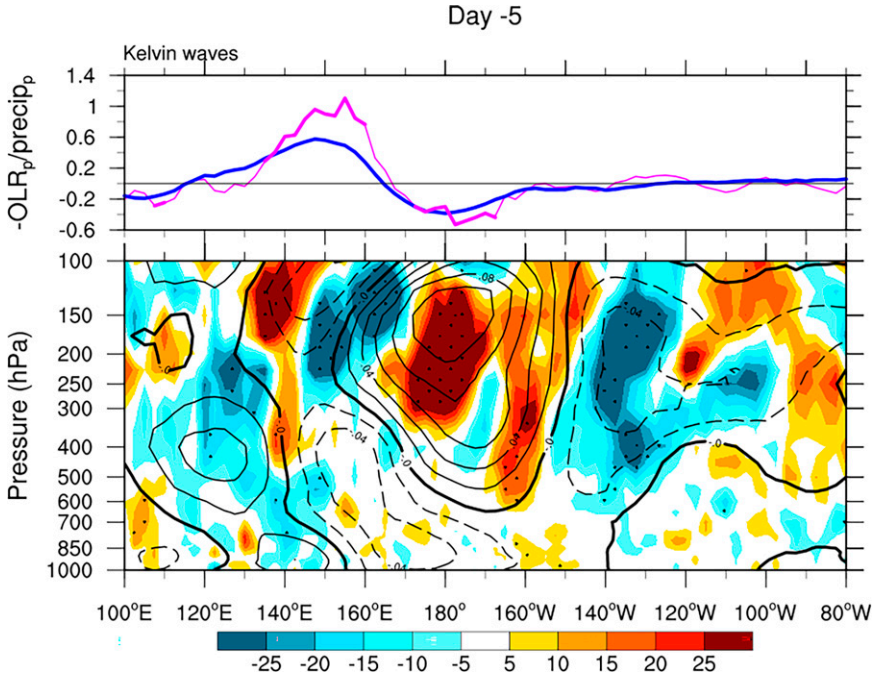

FIG. 8. Zonal–height cross section of anomalous meridionally projected zonal wind (u_p; contours) and momentum flux forcing (F_p; colors) regressed onto PC1 of the Kelvin wave EOF during JJA for day −5. Meridionally projected OLR (OLR$_p$; blue) and TRMM precipitation (precip$_p$; magenta) are also plotted at the top panel. The u_p is contoured every 2×10^{-2} m s^{-1} with zero lines thickened and negative values dashed. Momentum flux forcing F_p is shaded in 10^{-8} m s^{-2}. OLR$_p$ (W m^{-2}) and precip$_p$ (mm h^{-1}) are multiplied by a factor of −1 and 80 respectively for plotting purposes. Only statistically significant u_p at the 95% interval is plotted. Statistically significant OLR$_p$ and precip$_p$ at the 95% interval is thickened. Stippling shows F_p statistically significant at the 90% interval.

presumably due to extratropical eddies encountering the exit region of the subtropical jet (Fig. 1a).

Figure 8 shows the longitude–height cross section of u_p (contours) and F_p (colors) for the Kelvin wave on day −5. The zonal wind tilts westward with height throughout the troposphere and eastward in the stratosphere, with maxima in the upper and lower troposphere as reported in previous studies (e.g., Straub and Kiladis 2002; Kiladis et al. 2009). The familiar Kelvin wave structure indicates that the meridional projection of zonal wind indeed is able to isolate Kelvin wave signal over the Pacific during this time of the year. The momentum flux forcing peaks between 150 and 200 hPa where equatorward propagation of Rossby waves is most prominent (Hoskins et al. 1983). The forcing is collocated with the strongest zonal winds of the Kelvin wave. This nearly in-phase relationship indicates that the momentum flux forcing is most effective in generating EKE in the upper troposphere.

c. *Cospectrum between F_p and u_p*

We have shown that the momentum flux forcing projects onto the Kelvin wave meridional structure and that they have similar phase speeds (Fig. 7). To provide further evidence of resonance due to their similar frequencies, we examine the cospectrum between u_p and F_p, which conveys their covariance in the wavenumber–frequency domain. Conceptually, positive covariance between F_p and u_p represents the generation of EKE in Fourier space, without any filtering or compositing such as in Figs. 7 and 8. Figure 9 shows EKE generation peaks near the Kelvin wave dispersion line, consistent with the spectral peak in OLR (Fig. 2a) and the zonal scale and period of Kelvin waves isolated in the EOF analysis (Fig. 4). This result supports the notion that the Kelvin waves are energetically maintained by the momentum flux forcing. While the extratropical disturbances span a relatively broad range of zonal wavenumbers and frequencies (Fig. 2c), it is the forcing with similar spatial and temporal scales that project onto the meridional structure of the Kelvin mode that leads to its excitation and maintenance.

It is worth further clarifying how we interpret the phase relationship between u_p and F_p. When one variable leads the other by a quarter of a phase, it is tempting to interpret the former as the "cause" for the latter due to its earlier appearance in time. However, since the covariance of the two is zero due to their quadrature relationship, the leading variable cannot contribute to the energy generation [Eq. (3)]. Rather, it acts to propagate and develop the lagging variable (Sakaeda and Roundy 2014; Matthews 2021). For resonance to occur, the two must be at least partially in phase such that the forcing can cause

Brought to you by NOAA Central Library | Unauthenticated | Downloaded 07/19/23 06:04 PM UTC

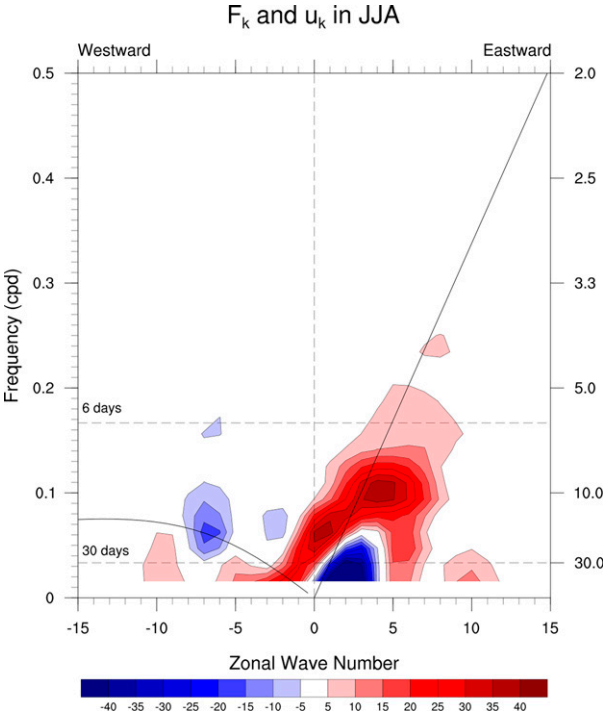

FIG. 9. Cospectrum of meridionally projected momentum flux convergence (F_p) and zonal wind (u_p) at 200 hPa over 120°E–140°W in JJA. Spectral power has a unit of 10^{-11} m^2 s^{-2}. A positive cospectrum indicates an in-phase relationship between the two variables while a negative one denotes an out-of-phase relationship.

amplification. This is indeed what is seen in the cospectrum where F_p and u_p are in phase, and therefore F_p amplifies and maintains u_p. This distinction between propagation and amplification will be further investigated in the next section.

d. Comparison with linear terms

While the above results provide strong evidence that the forcing term F contributes to both the triggering and maintenance of Kelvin waves over the Pacific, a related question concerns the role of other source terms on the right-hand side of Eq. (1). To address this question, a full momentum budget analysis was performed by calculating each of the terms in Eq. (1) and then grouping together the linear source terms (denoted L) as the counterpart to the nonlinear term F. The resulting budget quantities (including the residual R) were then cast in the Kelvin-projected composite framework of Fig. 7, using the same regression approach as described previously. Finally, to assess the relative contributions of L_p versus F_p toward promoting the eastward propagation and maintenance of fluctuations in u_p, the following bulk quantities were calculated:

$$S_p = \frac{\left\| \left(\frac{\partial u_p'}{\partial t} \right) x_p' \right\|}{\left\| \left(\frac{\partial u_p'}{\partial t} \right) \left(\frac{\partial u_p'}{\partial t} \right) \right\|} \quad \text{and}$$

$$S_m = \frac{\|u_p' x_p'\|}{\|u_p' u_p'\|},$$

where x_p corresponds to an individual meridionally projected term in the budget, primes denote regressed anomalies, and "$\|\cdot\|$" denotes integration over time (from days −8 to +4) and longitude (120°E–140°W). Because S_p depends on the product of x_p' and $\partial u_p'/\partial t$, it provides a bulk measure of the contribution of x_p' to the eastward propagation of fluctuations in u_p'. Conversely, the dependence of S_m on the product of x_p' and u_p' means that it provides a bulk measure of the contribution of x_p' to the maintenance of u_p' (i.e., EKE). The motivation for this approach comes from previous studies that have used it to

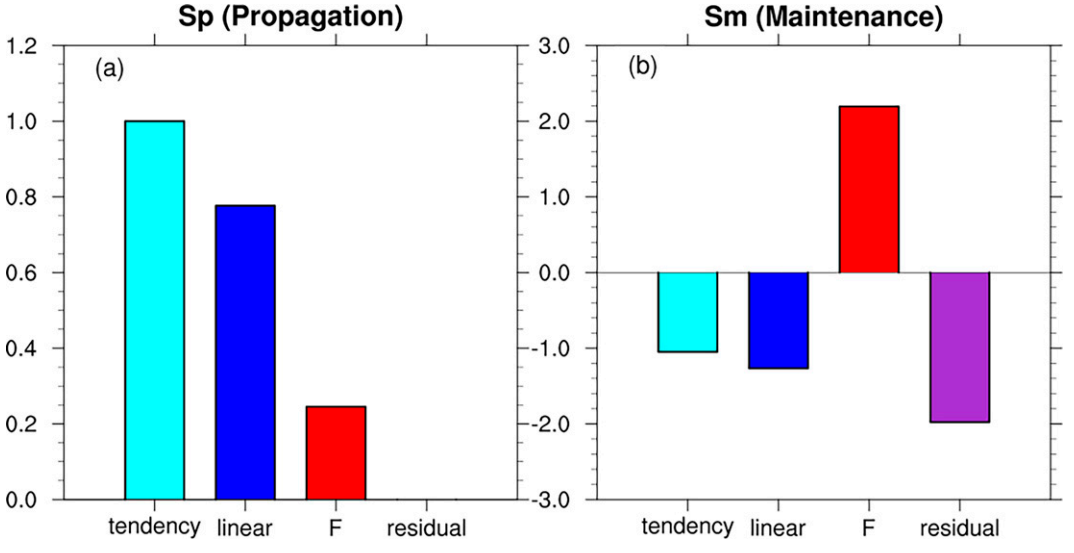

FIG. 10. Fractional contribution of each term to the (a) propagation (S_p) and (b) maintenance (S_m) of the zonal wind perturbations u_p' for Kelvin waves in JJA. Terms plotted in each panel are, from left to right, the tendency of u_p', linear source terms combined L_p', nonlinear momentum flux forcing F_p', and the residual R_p'. Both terms are dimensionless, with S_m expressed in 10^{-6}. See text of Fig. 10 for details.

Brought to you by NOAA Central Library | Unauthenticated | Downloaded 07/19/23 06:04 PM UTC

look at how various processes contribute to the propagation and maintenance of the MJO in terms of moisture and/or moist static energy (e.g., Andersen and Kuang 2012; Ren et al. 2021).

Figure 10 shows S_p and S_m for the time tendency of u'_p, linear terms combined L'_p, nonlinear momentum flux forcing F'_p, and the residual R'_p. The results shown here are not sensitive to the time and longitude where the integration is calculated. By definition, S_p is 1 for the zonal wind tendency. The residual for propagation is less than 0.03, indicating the budget closes reasonably well. The blue bars in Fig. 10 show that while linear processes (L'_p) contribute significantly to the propagation of the Kelvin wave's zonal wind anomalies (as might be expected on the basis of linear wave theory), they also act to damp these anomalies. In contrast, the nonlinear forcing F'_p (red bars) is shown to be essential for wave maintenance, while also providing a modest contribution to propagation. The interpretation is thus that the wave is indeed a linear mode of the tropical atmosphere that is resonantly forced by the extratropics. One caveat is that the residual R'_p provides a substantial negative contribution to wave maintenance, which may be partly attributed to the effects of dissipation not explicitly accounted for in the budget analysis.

e. Discussion

To summarize, the mechanism of resonance in which extratropical Rossby waves excite tropical circulation in equatorial easterlies is understood as follows: the extratropical forcing is manifested as momentum flux forcing F, due to Rossby waves encountering mean equatorial easterlies and their critical lines. This remote forcing acts on the poleward flank of Kelvin wave's meridional eigenstructure, which is estimated using meridional projected F_p and u_p. The F_p and u_p share similar zonal wavenumbers, frequencies, and phase speeds, in accordance with the idea of wave resonance. Generation of Kelvin wave EKE is evidenced by the positive covariance between F_p and u_p. The divergence and convergence of the zonal wind, in turn, help to drive the convective signals of the Kelvin wave.

The circulation and forcing mechanism outlined above is broadly similar to the simulation results from TK21. The forcing F drives zonal wind perturbations as well as EKE. At the same time, tropical convection can also act as a source of Rossby wave energy in the subtropics (e.g., Sardeshmukh and Hoskins 1988), so the forcing F may involve more than just the effects of "external" eddies impinging on the tropics from higher latitudes. In Fig. 4, for example, the subtropical gyre moving along 20°S east of the date line appears to be partly driven by the Kelvin wave's convective outflow. This issue was addressed in TK21 using a mechanism denial experiment. In particular, they conducted a simulation where the effects of extratropical eddies were actively suppressed. In that case, the Kelvin wave activity and EKE were seen to be significantly reduced at zonal wavenumbers 3–5 (see their Figs. 14 and 15). Taken together with the observational analysis here, these results demonstrate how extratropical Rossby waves can act to drive moist Kelvin waves through momentum flux forcing and resonance under suitable background flow conditions (i.e., a relatively strong subtropical jet, together with modest easterlies at the equator).

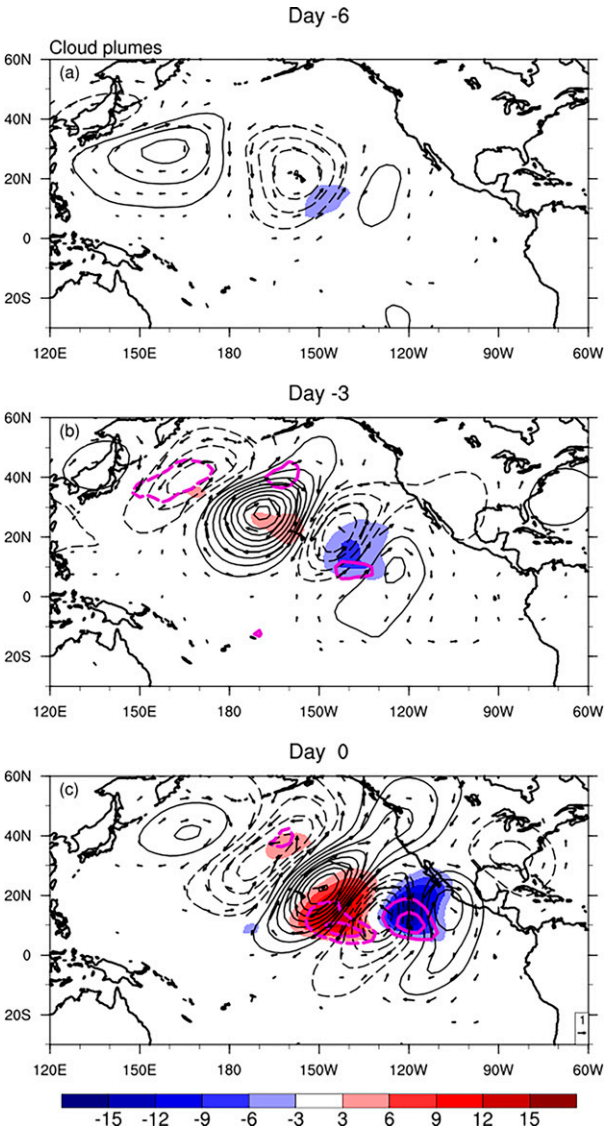

FIG. 11. As in Fig. 6, but for the cloud plumes. Anomalous OLR (colors; W m^{-2}), 200-hPa streamfunction (black contours), wind vectors (vectors), and GPM IMERG precipitation (magenta contours) regressed onto PC1 of the cloud plume EOF during DJF for days (a) −6, (b) −3, and (c) 0. Streamfunction is contoured every 6×10^5 m^2 s^{-1} in black with zero lines omitted. GMP-IMERG precipitation is contoured every 0.05 mm h^{-1} in magenta with zero lines omitted. A reference wind vector of 1 m s^{-1} is shown in the bottom-right corner. Only fields that are statistically significant at the 95% interval are shown.

5. Local pathway: Eastward-moving tropical cloud plumes

a. Extratropical Rossby waves

We now turn to the local pathway where the mean basic state allows extratropical Rossby waves to intrude into the tropics through westerly ducts. Figure 11 shows the first EOF of eastward 2–20-day filtered OLR and the associated

Brought to you by NOAA Central Library | Unauthenticated | Downloaded 07/19/23 06:04 PM UTC

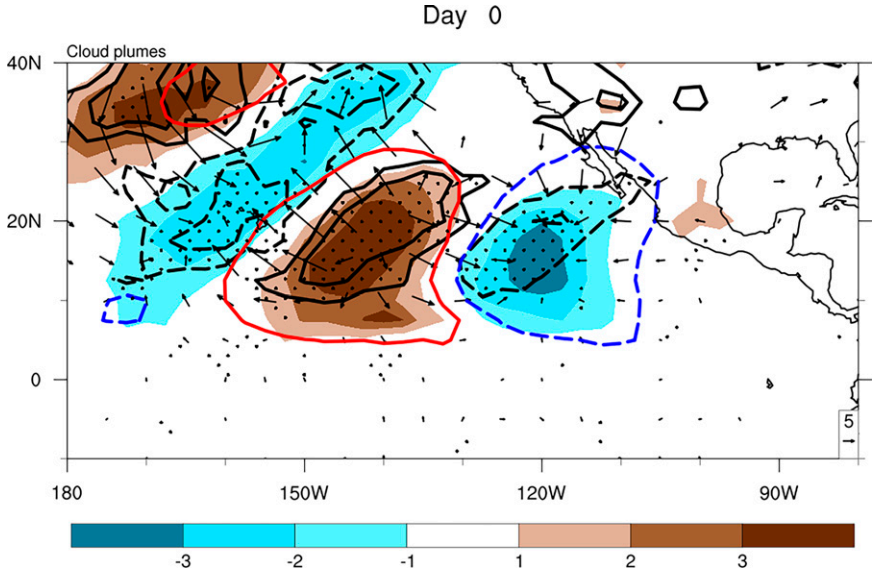

FIG. 12. As in Fig. 5, but for the cloud plumes. Anomalous 350-hPa ω (colors; 10^{-2} Pa s^{-1}) and **Q** vectors (vectors); **Q** vector divergence regressed onto PC1 of the cloud plume EOF during DJF for day 0. The **Q** vector divergence is contoured every 1.5×10^{-17} Pa^{-1} s^{-3} with negative values (convergence) dashed and zero lines omitted. A reference **Q** vector of 5×10^{-12} m Pa^{-1} s^{-3} is shown in the bottom-right corner. For reference, the anomalous OLR at ± 3 W m^{-2} is also overlaid. Fields are drawn only when they are statistically significant at the 95% interval except for the **Q** vector convergence where stippling indicates the 90% level.

circulations. The EOF depicts alternating cloud patterns extending from the tropics to the subtropics (Fig. 11c). The first two EOFs describe similar southwest–northeast oriented patterns and the two together explain over 15% of the variance. Their associated PCs are correlated at 0.7 at a 1-day lag and the two EOFs constitute an eastward-propagating pair with a period of 4 days.

Figure 11 depicts the typical evolution of the tropical cloud plume. Cloudiness develops in the southwesterly flow ahead of the trough, although most of the cloudiness is nonprecipitating with the exception of a narrow strip along the ITCZ (magenta lines in Fig. 11). The positively tilted circulations indicate poleward westerly momentum transport and equatorward energy propagation. Although these disturbances are often characterized by anticyclonic wave breaking due to their large amplitude (Shapiro et al. 2001; Funatsu and Waugh 2008; Ryoo et al. 2013), their energy dispersion as well as wave propagation can be largely explained by linear Rossby wave theory (K98; Matthews and Kiladis 1999a,b). These eastward-propagating circulations and cloud features are also referred to as "extratropical intrusion" or "potential vorticity streamers" in the literature (e.g., K98; HSK20; Mcguirk et al. 1987; Iskenderian 1995; Tomas and Webster 1994; Knippertz 2005; Fröhlich et al. 2013).

Rossby waves in a westerly duct are typically accompanied by strong temperature and vorticity advection (K98), which contribute to QG forcing. Figure 12 shows the anomalous **Q** vectors and their divergence at 350 hPa, near the level of maximum vertical motion. Regions of **Q** vector convergence match where there is upward motion and high cloud tops. The strong correspondence indicates that dynamical forcing is responsible for the upward motion and cloudiness in the region. An examination of the latitude–height cross section of the **Q** vector divergence (Fig. 13) reveals that the QG forcing is limited to levels above 500 hPa and poleward of 10°N. The low-level trade winds create an "easterly dome" and a critical level in the midtroposphere, which prevents the Rossby waves from further propagating equatorward and downward (Tomas and Webster 1994). Although the extratropical waves are confined to the upper levels where the westerly duct resides, their associated forcing is still able to destabilize the column and trigger convection within the ITCZ (K98; Funatsu and Waugh 2008).

The eastward-moving cloud plume maintains an extratropical vertical structure distinct from observed moist Kelvin waves. The meridionally projected zonal wind u_p is shown in Fig. 14 (see also Fig. 9 of HSK20). The u_p tilts westward with height below 600 hPa and eastward above. The eastward tilt is associated with heat transport and can be explained by kinematics in geostrophically balanced circulations (e.g., James 1994):

$$v_g = \frac{1}{f}\frac{\partial \phi'}{\partial x},$$

$$T' = H\frac{\partial \phi'}{\partial z},$$

where ϕ denotes geopotential, f is the Coriolis parameter, R is the gas constant, T is temperature, $z = -H\ln(p/p_0)$ is pseudoheight, H is scale height, and p is pressure. Assume ϕ' has a

Brought to you by NOAA Central Library | Unauthenticated | Downloaded 07/19/23 06:04 PM UTC

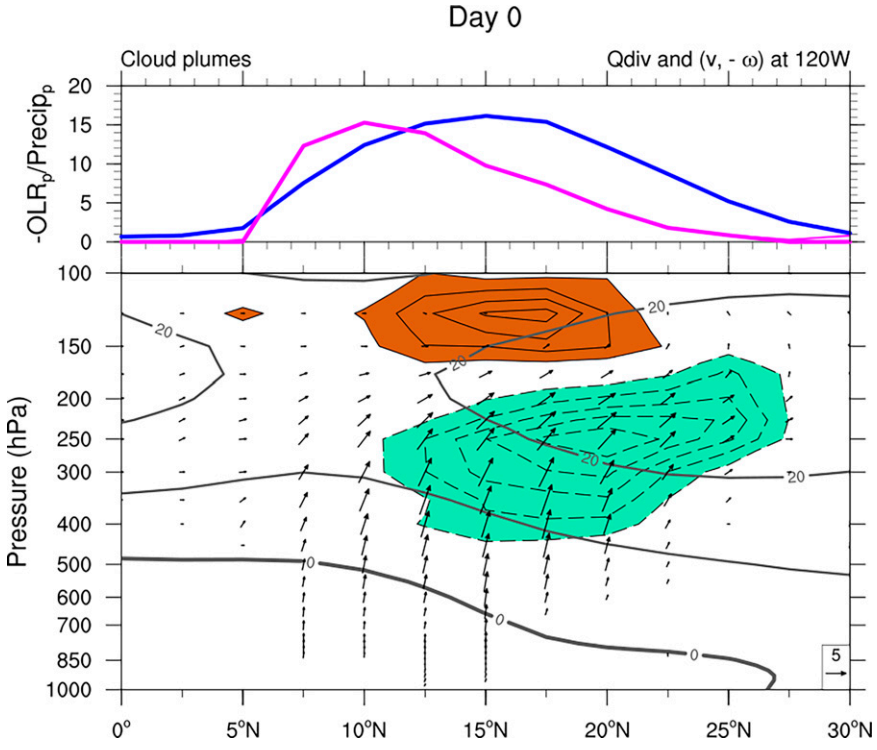

FIG. 13. Latitude–height cross section of anomalous **Q** vector divergence (black contours) and meridional and vertical pressure velocity (vectors) regressed onto PC1 of the cloud plume EOF during DJF at 120°W for day 0. The **Q** vector convergence and divergence (10^{-17} Pa^{-1} s^{-3}) are shaded green and brown, respectively. The associated OLR and GPM IMERG precipitation is plotted in the top panel for reference. The vertical pressure velocity is multiplied by −100 for plotting purposes. Climatological zonal wind (m s^{-1}) between 180° and 80°W is also overlaid in gray. Only fields that are statistically significant at the 95% interval are shown.

sinusoidal solution of the form $\phi' = A\sin(kx + mz)$ where A is the amplitude of the wave and k and m the zonal and vertical wavenumbers, with positive k and m representing eastward- and upward-propagating disturbances. The heat flux is expressed as $\overline{v_g T'} \propto km$. Since the net heat transport by these disturbances is equatorward (negative; dashed lines in Fig. 1d) the vertical wavenumber of these eastward propagating waves ($k > 0$) is also negative. The phase lines therefore tilt eastward with height, inconsistent with a Kelvin wave structure (cf. Fig. 8). This vertical structure reflects the fact that Rossby waves maintain their baroclinic characteristics. This result also highlights the fact that the projection is only a meridional decomposition and does not necessarily guarantee that a Kelvin wave is active. Further information pertaining to the zonal and vertical structures of the disturbance, including the phasing between the wind and mass fields, is also needed to make this determination.

b. *Momentum flux forcing*

The cloud plumes are typically associated with anticyclonic wave breaking. Therefore, despite their occurrence in the westerly duct, they have substantial nonlinear momentum flux forcing in the mid-to-upper troposphere (colors in Fig. 14). Figure 15 shows signals in F_p and u_p moving in tandem at roughly 8 m s^{-1}, much slower than typical Kelvin waves at 15–20 m s^{-1}, which again is inconsistent with the existence of Kelvin waves in this region during DJF. The forcing leads the zonal wind by roughly a quarter wave cycle, as opposed to being in phase with one another in Kelvin waves (Fig. 7). The implication is that nonlinear processes also contribute to the driving of cloud-plume convection, through forcing of divergent upper-level zonal wind anomalies. The crucial role of this forcing, as compared to the linear source term L_p, is made clear in Fig. 16. As conveyed by the integral quantities S_p and S_m, Fig. 16 shows how F_p is essential for fostering both the propagation and maintenance of eastward-moving signals in u_p. The fact that L_p provides only a nominal contribution to propagation is quite different from what was found in the Kelvin wave case (Fig. 10), where L_p was by far the leading contributor. Thus, rather than being a linear mode of the tropics, it appears that tropical cloud plumes should be regarded as a mode of variability that is entirely forced by the extratropics.

6. Summary and discussion

The extratropical forcing of tropical circulations was investigated for the period 1979–2019 using satellite-derived OLR and ERA5 reanalysis data in the context of two distinct types

Brought to you by NOAA Central Library | Unauthenticated | Downloaded 07/19/23 06:04 PM UTC

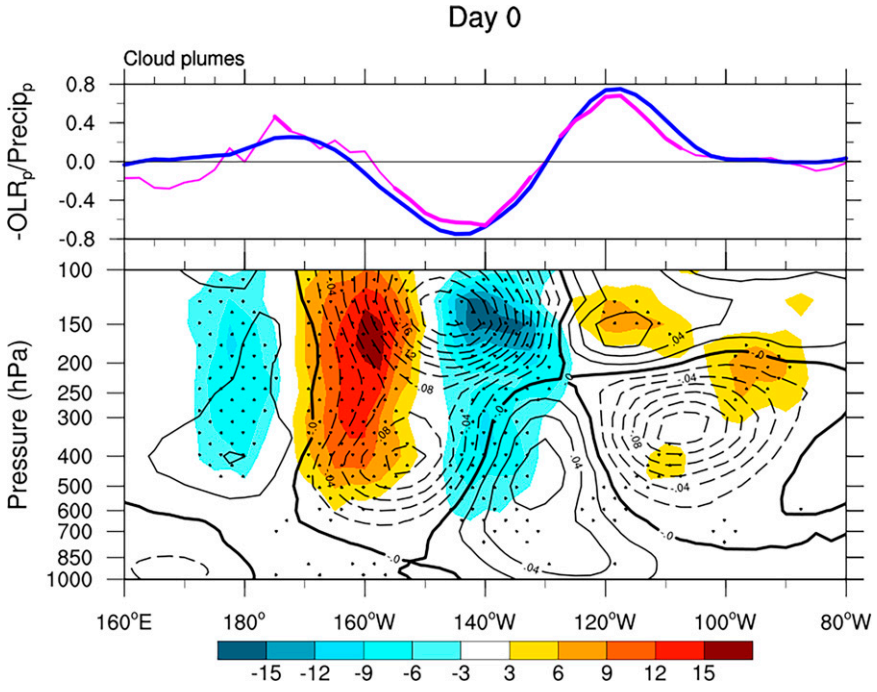

FIG. 14. As in Fig. 8, but for the cloud plumes. Zonal–height cross section of anomalous meridionally projected zonal wind (u_p; contours) and momentum flux forcing (F_p; colors) regressed onto PC1 of the cloud plume EOF during DJF for day 0. Meridionally projected OLR (OLR$_p$) and GPM IMERG precipitation (precip$_p$) are also plotted at the top panel. Note that u_p is contoured every 2×10^{-2} m s^{-1} with zero lines thickened and negative values dashed; F_p is shaded in 10^{-7} m s^{-2}; OLR$_p$ (W m^{-2}) and precip$_p$ (mm h^{-1}) are multiplied by a factor of -1 and 80 respectively for plotting purposes. Only statistically significant u_p at the 95% interval is plotted. Statistically significant OLR$_p$ and precip$_p$ at the 95% interval is thickened. Stippling shows F_p statistically significant at the 90% interval.

of tropical disturbances: convectively coupled Kelvin waves (Kelvin waves) over the west-central Pacific during JJA and eastward-moving cloud plumes over the east Pacific during DJF. As illustrated by the schematic in Fig. 17, the dominant forcing pathway in the two cases was found to be quite different, owing to differences in the meridional structure of the background zonal flow.

In the JJA case, the presence of equatorial mean easterlies prevents the intrusion of extratropical eddies, such that their associated quasigeostrophic (QG) forcing of upward motion remains far removed from the tropics and thus cannot explain the observed excitation of Kelvin waves (Figs. 4 and 5). Rather, the excitation occurs via "resonance" between the tropical and extratropical circulations, as proposed in previous modeling studies. We demonstrated that in this "remote" pathway, the extratropical forcing is manifested as eddy momentum flux forcing (F), due to equatorward-propagating Rossby waves encountering a critical line in the subtropical upper troposphere (Figs. 3 and 6). This remote eddy forcing acts on the poleward flanks of the Kelvin wave's meridional eigenstructure, as evidenced by meridional projection of anomalies in the forcing and zonal wind. The forcing F_p and attendant Kelvin waves (u_p) share similar wavenumber, frequency, and phase speeds, consistent with the idea of wave resonance between the tropics and extratropics (Figs. 7 and 9). The in-phase relationship, or positive covariance between the two variables, indicates generation of EKE [Eq. (3)], as expected from a resonantly forced disturbances with growing amplitude (Figs. 7–9). The nonlinear F_p is the leading contributor to the maintenance and amplification of Kelvin waves (Fig. 10). The increase in zonal EKE is thought to favor upper-level divergence and enhance convective activity. Meanwhile, propagation of the disturbance is driven mainly by linear terms due to the linear dynamics of an equatorial mode, but those linear processes also act to damp the disturbance via destruction of EKE (Fig. 10).

In contrast, in the DJF case, a westerly duct allows extratropical Rossby waves to intrude into the tropics where they then act to excite eastward-moving cloud plumes (Fig. 11) through local QG forcing (Figs. 12 and 13), as well as nonlinear momentum flux forcing due to wave breaking (Figs. 3, 14, and 15). The entirely forced nature of these disturbances (as opposed to being resonant linear modes of the tropics) is evidenced by the fact that linear dynamics plays virtually no role in the propagation or maintenance of their meridionally projected zonal wind anomalies (Fig. 16), unlike what is true for Kelvin waves during JJA.

Brought to you by NOAA Central Library | Unauthenticated | Downloaded 07/19/23 06:04 PM UTC

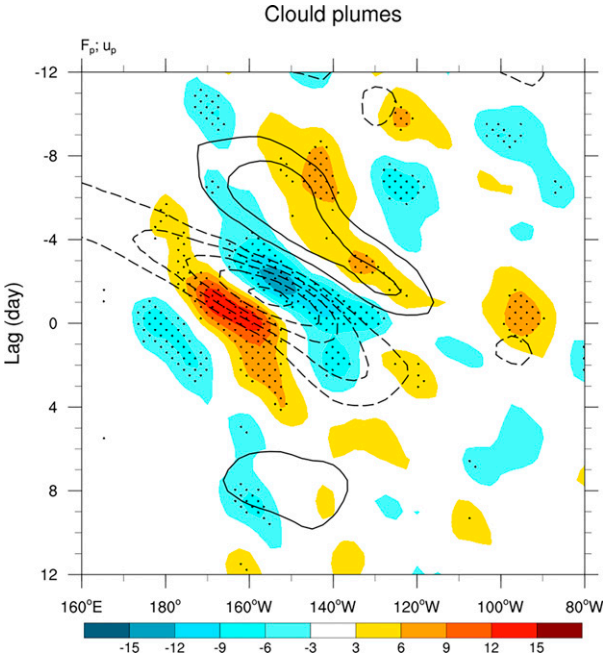

FIG. 15. As in Fig. 7, but for the cloud plumes. Hovmöller diagram of anomalous meridionally projected zonal wind (u_p; contours) and momentum flux forcing (F_p, colors) at 200 hPa regressed onto PC1 of the cloud plume EOF during DJF. The u_p is contoured every 3×10^{-2} m s^{-1} with zero lines omitted; negative values are dashed; F_p is shaded in 10^{-7} m s^{-2}. Only statistically significant u_p at the 95% interval is plotted. Stippling shows statistically significant forcing F_p at the 90% interval.

The phenomenon whereby midlatitude forcing affects tropical circulations in equatorial easterlies has long been understood on the basis of modeling studies as a resonant interaction between the tropics and extratropics. The current study documented the nature of this interaction in the real world, which entails Rossby waves encountering a critical line that results in the excitation of equatorial wave modes, via momentum flux forcing acting on their poleward flanks. This remote forcing pathway, which was documented herein for the first time using observations, is consistent with the simulation results in TK21, whose set of experiments further established the critical dependence of such forcing on the meridional structure of the background zonal flow. While other factors may also be involved, this mean flow dependence is presumably at the heart of the explanation for why Kelvin waves are generally inactive in the DJF case, since the speed of the remote eddy forcing there is generally too slow to resonantly excite Kelvin waves, as evidenced in Figs. 2 and 3 and discussed in section 3c.

While it is beyond the scope of current study, it appears that the eddy momentum flux forcing may generally be more effective than the mass and heat flux forcing of QG dynamics in exciting equatorial waves [see also the dry modeling study of Hoskins and Yang (2000)]. The reason is that the QG forcing appears to mainly drive vertical motion locally at the extratropical Rossby wave scale, as opposed to resonantly projecting onto any sort of equatorial eigenstructure. Of course, equatorial waves can also arise from other "external" forcing mechanisms outside of the tropics such as the passage of cold air outbreaks and pressure surges (Chang and Lau 1980; Compo et al. 1999; Liebmann et al. 2009), as well as internal mechanisms within the tropics, such as stratiform instability and wind-induced surface heat exchange (Straub and Kiladis 2003b). Further investigation is needed to evaluate the efficiency of these various mechanisms and forcing pathways.

The eddy momentum flux forcing could also be important for the excitation and maintenance of intraseasonal variability (Fig. 9). This potential pathway is consistent with previous studies (e.g., Ray and Zhang 2010; Sakaeda and Roundy 2014, 2015, 2016; Adames et al. 2014) but demands further

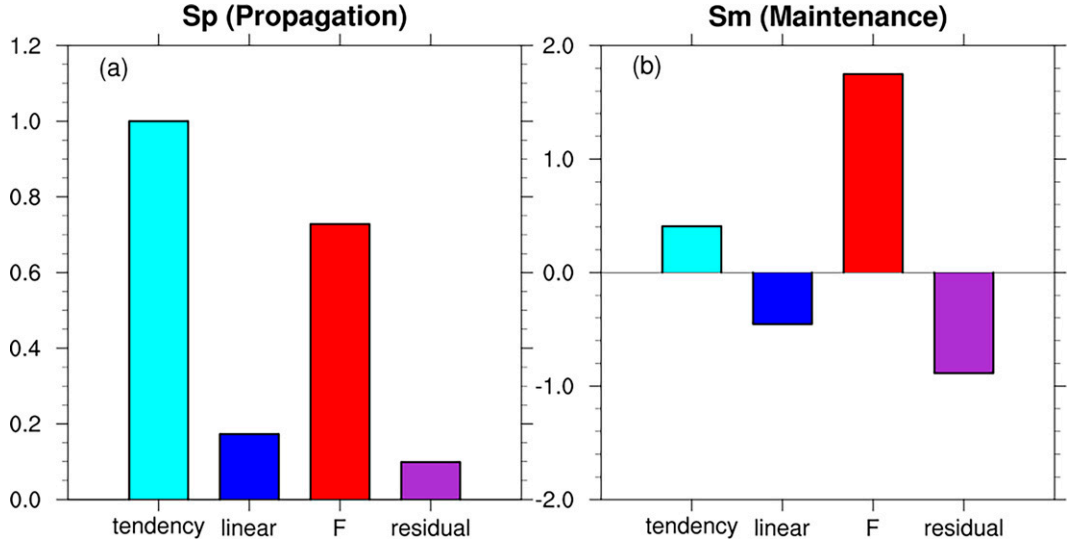

FIG. 16. As in Fig. 10, but for the cloud plumes. Fractional contribution of each term to the (a) propagation (S_p) and (b) maintenance (S_m) of the zonal wind perturbations u'_p for the cloud plumes in DJF. Terms plotted in each panel are, from left to right, the tendency of u'_p, linear source terms combined L'_p, nonlinear momentum flux forcing F'_p, and the residual R'_p. Both terms are dimensionless, with S_m expressed in 10^{-6}.

Brought to you by NOAA Central Library | Unauthenticated | Downloaded 07/19/23 06:04 PM UTC

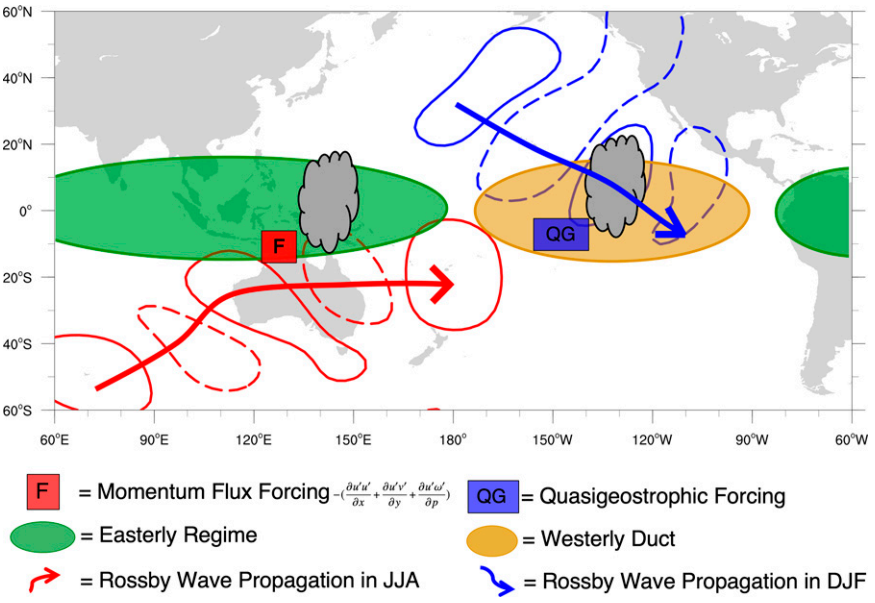

FIG. 17. A schematic summarizing the two extratropical pathways to forcing tropical convection investigated in this study. The cartoon clouds denote regions where tropical convection is excited. In the easterly region, Rossby waves encounter the critical line, generate momentum flux forcing (*F*), and excite Kelvin waves through resonance. On the contrary, Rossby waves intrude into the tropics in the westerly duct and trigger cloud plumes, mainly by quasigeostrophic (QG) forcing. See text in section 6 for more details.

investigation, since both local and external mechanisms may be relevant, due to different basic states across basins. In addition, tropical variability, particularly over the east Pacific, is sensitive to the subtropical jet and storm tracks modulated by the MJO and the ENSO (Matthews and Kiladis 1999a,b; Straub and Kiladis 2003a; Shapiro et al. 2001; Ryoo et al. 2013). The warm phase of ENSO, for example, may favor the resonant forcing of Kelvin waves in the east Pacific due to the extension of the subtropical jet and weakening of the westerly duct, which can be investigated using the diagnostics developed here. Further studies on the variability of equatorial waves in relation to tropical–extratropical interactions are warranted, since the problem is known to have an important bearing on the challenge of subseasonal to seasonal prediction (Stan et al. 2017; Dias et al. 2018).

Acknowledgments. We thank Pragallva Barpanda, Maria Gehne, and Brandon Wolding for their input on this study. We also thank Cristiana Stan and two anonymous reviewers whose comments greatly improved the manuscript. Y.-M. Cheng is grateful for the postdoc opportunity supported by NOAA and National Research Council. S. Tulich acknowledges support from the NSF through the award AGS-1839471.

Data availability statement. The OLR data are available at NOAA Physical Sciences Laboratory website. The GPM IMERG and TRMM precipitation can be downloaded at NASA Earth Data website. The ERA5 reanalysis data can be accessed through the ECMWF website.

APPENDIX

Determination of Trapping Scale

The trapping scale ϕ_0 is a parameter that determines the meridional scale of the equatorial wave (section 2h). Following TK21, we adopted an empirical method based on a multivariate EOF to determine this scale. We used OLR and the zonal component of the divergent wind at 200 hPa in JJA to represent convectively coupled Kelvin waves. Both OLR and zonal divergent wind show a significant spectral peak along Kelvin dispersion and the coherence between the two is over 0.45 (not shown). We then filtered both variables to retain the Kelvin wave band using standard wavenumber–frequency method (Wheeler and Kiladis 1999). After filtering, each field was normalized by its standard deviation within the domain to ensure equal contribution to the variance of the combined matrix (Wheeler and Hendon 2004). The zonal boundaries of the domain were 120°E–140°W, consistent with the Kelvin wave EOF, and the meridional bounds are 15°S–15°N.

To extract the meridional structure of Kelvin waves, a matrix is formulated as a spatial domain over latitude with sampling domain of time and longitude. The resultant EOFs have a latitudinal structure between 15°S and 15°N and their PCs measure the amplitude of this structure at each time and longitude. We can then represent the meridional structure of Kelvin waves by regressing raw data against the PCs to reconstruct a meridional profile of Kelvin waves from pole to pole. Note that this meridional multivariate EOF is different from the EOF analysis in section 2b where the structure domain is

Brought to you by NOAA Central Library | Unauthenticated | Downloaded 07/19/23 06:04 PM UTC

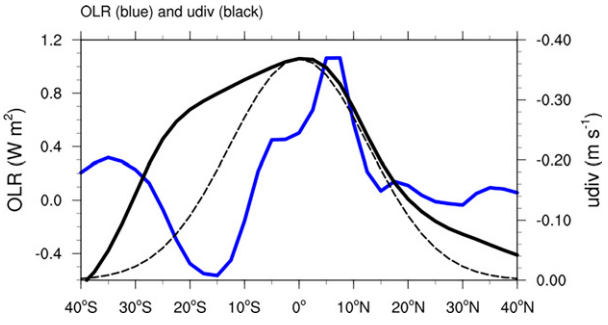

FIG. A1. Regressed OLR and 200-hPa zonal divergent wind structure associated with a multivariate EOF of Kelvin-filtered OLR and 200-hPa zonal wind. The EOF is calculated using data from 15°S–15°N, 120°E–140°W in JJA. The dashed lines are parabolic cylinder functions with a trapping scale of 9° (black).

latitude and longitude and the sampling domain is time. Those EOFs describe structures on a map with PCs measuring amplitude of those patterns at each time.

Figure A1 shows the regressed meridional structure of Kelvin waves in OLR (blue) and zonal divergent wind (black). The leading EOF structure explains 39.9% of the total variance. The OLR peaks off the equator, as expected from the mean position of the ITCZ during this time of the year. The zonal divergent wind, on the contrary, is nearly centered at the equator, consistent with the theoretical Kelvin wave structure. It is not, however, symmetric about the equator. The "shoulder" south of 15°S is due to the extratropical storm tracks. In fact, our tests using less restrictive filters and winds, such as an eastward filter and total zonal wind, demonstrate an even more pronounced shoulder in the Southern Hemisphere (not shown). This indicates that part of the zonal wind variance in the equatorial region is linked to the extratropical disturbances.

REFERENCES

Adames, A. F., J. Patoux, and R. C. Foster, 2014: The contribution of extratropical waves to the MJO wind field. *J. Atmos. Sci.*, **71**, 155–176, https://doi.org/10.1175/JAS-D-13-084.1.

Andersen, J. A., and Z. Kuang, 2012: Moist static energy budget of MJO-like disturbances in the atmosphere of a zonally symmetric aquaplanet. *J. Climate*, **25**, 2782–2804, https://doi.org/10.1175/JCLI-D-11-00168.1.

Bao, J.-W., S. A. Michelson, P. J. Neiman, F. M. Ralph, and J. M. Wilczak, 2006: Interpretation of enhanced integrated water vapor bands associated with extratropical cyclones: Their formation and connection to tropical moisture. *Mon. Wea. Rev.*, **134**, 1063–1080, https://doi.org/10.1175/MWR3123.1.

Baranowski, D. B., and Coauthors, 2020: Social-media and newspaper reports reveal large-scale meteorological drivers of floods on Sumatra. *Nat. Commun.*, **11**, 2503, https://doi.org/10.1038/s41467-020-16171-2.

Chang, C.-P., and K. M. W. Lau, 1980: Northeasterly cold surges and near-equatorial disturbances over the winter MONEX area during December 1974. Part II: Planetary-scale aspects. *Mon. Wea. Rev.*, **108**, 298–312, https://doi.org/10.1175/1520-0493(1980)108<0298:NCSANE>2.0.CO;2.

Charney, J. G., 1969: A further note on large-scale motions in the tropics. *J. Atmos. Sci.*, **26**, 182–185, https://doi.org/10.1175/1520-0469(1969)026<0182:AFNOLS>2.0.CO;2.

Cheng, Y.-M., C. D. Thorncroft, and G. N. Kiladis, 2019: Two contrasting African easterly wave behaviors. *J. Atmos. Sci.*, **76**, 1753–1768, https://doi.org/10.1175/JAS-D-18-0300.1.

Compo, G. P., G. N. Kiladis, and P. J. Webster, 1999: The horizontal and vertical structure of East Asian winter monsoon pressure surges. *Quart. J. Roy. Meteor. Soc.*, **125**, 29–54, https://doi.org/10.1002/qj.49712555304.

Das, U., and C. Pan, 2016: Equatorial atmospheric Kelvin waves during El Niño episodes and their effect on stratospheric QBO. *Sci. Total Environ.*, **544**, 908–918, https://doi.org/10.1016/j.scitotenv.2015.12.009.

Dee, D. P., and Coauthors, 2011: The ERA-Interim reanalysis: Configuration and performance of the data assimilation system. *Quart. J. Roy. Meteor. Soc.*, **137**, 553–597, https://doi.org/10.1002/qj.828.

Dias, J., and G. N. Kiladis, 2014: Influence of the basic state zonal flow on convectively coupled equatorial waves. *Geophys. Res. Lett.*, **41**, 6904–6913, https://doi.org/10.1002/2014GL061476.

——, M. Gehne, G. N. Kiladis, N. Sakaeda, P. Bechtold, and T. Haiden, 2018: Equatorial waves and the skill of NCEP and ECMWF numerical weather prediction systems. *Mon. Wea. Rev.*, **146**, 1763–1784, https://doi.org/10.1175/MWR-D-17-0362.1.

——, S. N. Tulich, M. Gehne, and G. N. Kiladis, 2021: Tropical origins of weeks 2–4 forecast errors during the Northern Hemisphere cool season. *Mon. Wea. Rev.*, **149**, 2975–2991, https://doi.org/10.1175/MWR-D-21-0020.1.

Fischer, M. S., B. H. Tang, and K. L. Corbosiero, 2017: Assessing the influence of upper-tropospheric troughs on tropical cyclone intensification rates after genesis. *Mon. Wea. Rev.*, **145**, 1295–1313, https://doi.org/10.1175/MWR-D-16-0275.1.

Fröhlich, L., P. Knippertz, A. H. Fink, and E. Hohberger, 2013: An objective climatology of tropical plumes. *J. Climate*, **26**, 5044–5060, https://doi.org/10.1175/JCLI-D-12-00351.1.

Funatsu, B. M., and D. W. Waugh, 2008: Connections between potential vorticity intrusions and convection in the eastern tropical Pacific. *J. Atmos. Sci.*, **65**, 987–1002, https://doi.org/10.1175/2007JAS2248.1.

Gehne, M., and R. Kleeman, 2012: Spectral analysis of tropical atmospheric dynamical variables using a linear shallow-water modal decomposition. *J. Atmos. Sci.*, **69**, 2300–2316, https://doi.org/10.1175/JAS-D-10-05008.1.

Gill, A. E., 1980: Some simple solutions for heat-induced tropical circulation. *Quart. J. Roy. Meteor. Soc.*, **106**, 447–462, https://doi.org/10.1002/qj.49710644905.

Guo, Y., X. Jiang, and D. E. Waliser, 2014: Modulation of the convectively coupled Kelvin waves over South America and the tropical Atlantic Ocean in association with the Madden–Julian oscillation. *J. Atmos. Sci.*, **71**, 1371–1388, https://doi.org/10.1175/JAS-D-13-0215.1.

Haertel, P., 2021: Kelvin/Rossby wave partition of Madden–Julian oscillation circulations. *Climate*, **9**, 2, https://doi.org/10.3390/cli9010002.

Hendon, H. H., and M. C. Wheeler, 2008: Some space–time spectral analyses of tropical convection and planetary-scale waves. *J. Atmos. Sci.*, **65**, 2936–2948, https://doi.org/10.1175/2008JAS2675.1.

Brought to you by NOAA Central Library | Unauthenticated | Downloaded 07/19/23 06:04 PM UTC

Hersbach, H., and Coauthors, 2020: The ERA5 global reanalysis. *Quart. J. Roy. Meteor. Soc.*, **146**, 1999–2049, https://doi.org/10.1002/qj.3803.

Hoskins, B. J., and D. J. Karoly, 1981: The steady linear response of a spherical atmosphere to thermal and orographic forcing. *J. Atmos. Sci.*, **38**, 1179–1196, https://doi.org/10.1175/1520-0469(1981)038<1179:TSLROA>2.0.CO;2.

——, and G.-Y. Yang, 2000: The equatorial response to higher-latitude forcing. *J. Atmos. Sci.*, **57**, 1197–1213, https://doi.org/10.1175/1520-0469(2000)057<1197:TERTHL>2.0.CO;2.

——, I. Draghici, and H. C. Davies, 1978: A new look at the ω-equation. *Quart. J. Roy. Meteor. Soc.*, **104**, 31–38, https://doi.org/10.1002/qj.49710443903.

——, I. N. James, and G. H. White, 1983: The shape, propagation and mean-flow interaction of large-scale weather systems. *J. Atmos. Sci.*, **40**, 1595–1612, https://doi.org/10.1175/1520-0469(1983)040<1595:TSPAMF>2.0.CO;2.

Huaman, L., C. Schumacher, and G. N. Kiladis, 2020: Eastward-propagating disturbances in the tropical Pacific. *Mon. Wea. Rev.*, **148**, 3713–3728, https://doi.org/10.1175/MWR-D-20-0029.1.

Huang, P., and R. Huang, 2011: Climatology and interannual variability of convectively coupled equatorial waves activity. *J. Climate*, **24**, 4451–4465, https://doi.org/10.1175/2011JCLI4021.1.

Huffman, G. J., and Coauthors, 2007: The TRMM Multisatellite Precipitation Analysis (TMPA): Quasi-global, multiyear, combined-sensor precipitation estimates at fine scales. *J. Hydrometeor.*, **8**, 38–55, https://doi.org/10.1175/JHM560.1.

——, and Coauthors, 2020: Integrated multi-satellite retrievals for the global precipitation measurement (GPM) mission (IMERG). *Satellite Precipitation Measurement*, V. Levizzani et al., Eds., Springer, 343–353 pp., https://doi.org/10.1007/978-3-030-24568-9_19.

Iskenderian, H., 1995: A 10-year climatology of Northern Hemisphere tropical cloud plumes and their composite flow patterns. *J. Climate*, **8**, 1630–1637, https://doi.org/10.1175/1520-0442(1995)008<1630:AYCONH>2.0.CO;2.

James, I. N., 1994: *Introduction to Circulating Atmospheres*. Cambridge University Press, 448 pp.

Judt, F., 2020: Atmospheric predictability of the tropics, middle latitudes, and polar regions explored through global storm-resolving simulations. *J. Atmos. Sci.*, **77**, 257–276, https://doi.org/10.1175/JAS-D-19-0116.1.

Karoly, D. J., 1983: Rossby wave propagation in a barotropic atmosphere. *Dyn. Atmos. Oceans*, **7**, 111–125, https://doi.org/10.1016/0377-0265(83)90013-1.

Kiladis, G. N., 1998: Observations of Rossby waves linked to convection over the eastern tropical Pacific. *J. Atmos. Sci.*, **55**, 321–339, https://doi.org/10.1175/1520-0469(1998)055<0321:OORWLT>2.0.CO;2.

——, and K. M. Weickmann, 1992: Extratropical forcing of tropical Pacific convection during northern winter. *Mon. Wea. Rev.*, **120**, 1924–1939, https://doi.org/10.1175/1520-0493(1992)120<1924:EFOTPC>2.0.CO;2.

——, and M. Wheeler, 1995: Horizontal and vertical structure of observed tropospheric equatorial Rossby waves. *J. Geophys. Res.*, **100**, 22 981–22 997, https://doi.org/10.1029/95JD02415.

——, G. A. Meehl, and K. M. Weickmann, 1994: Large-scale circulation associated with westerly wind bursts and deep convection over the western equatorial Pacific. *J. Geophys. Res.*, **99**, 18 527–18 544, https://doi.org/10.1029/94JD01486.

——, C. D. Thorncroft, and N. M. J. Hall, 2006: Three-dimensional structure and dynamics of African easterly waves. Part I: Observations. *J. Atmos. Sci.*, **63**, 2212–2230, https://doi.org/10.1175/JAS3741.1.

——, M. C. Wheeler, P. T. Haertel, K. H. Straub, and P. E. Roundy, 2009: Convectively coupled equatorial waves. *Rev. Geophys.*, **47**, RG2003, https://doi.org/10.1029/2008RG000266.

——, J. Dias, and M. Gehne, 2016: The relationship between equatorial mixed Rossby–gravity and eastward inertio-gravity waves. Part I. *J. Atmos. Sci.*, **73**, 2123–2145, https://doi.org/10.1175/JAS-D-15-0230.1.

Knippertz, P., 2005: Tropical–extratropical interactions associated with an Atlantic tropical plume and subtropical jet streak. *Mon. Wea. Rev.*, **133**, 2759–2776, https://doi.org/10.1175/MWR2999.1.

——, 2007: Tropical–extratropical interactions related to upper-level troughs at low latitudes. *Dyn. Atmos. Oceans*, **43**, 36–62, https://doi.org/10.1016/j.dynatmoce.2006.06.003.

——, and Coauthors, 2022: The intricacies of identifying equatorial waves. *Quart. J. Roy. Meteor. Soc.*, **148**, 2814–2852, https://doi.org/10.1002/qj.4338.

Latos, B., and Coauthors, 2021: Equatorial waves triggering extreme rainfall and floods in southwest Sulawesi, Indonesia. *Mon. Wea. Rev.*, **149**, 1381–1401, https://doi.org/10.1175/MWR-D-20-0262.1.

Liebmann, B., and D. L. Hartmann, 1984: An observational study of tropical–midlatitude interaction on intraseasonal time scales during winter. *J. Atmos. Sci.*, **41**, 3333–3350, https://doi.org/10.1175/1520-0469(1984)041<3333:AOSOTI>2.0.CO;2.

——, and C. A. Smith, 1996: Description of a complete (interpolated) outgoing longwave radiation dataset. *Bull. Amer. Meteor. Soc.*, **77**, 1275–1277, https://doi.org/10.1175/1520-0477-77.6.1274.

——, G. N. Kiladis, L. M. V. Carvalho, C. Jones, C. S. Vera, I. Bladé, and D. Allured, 2009: Origin of convectively coupled Kelvin waves over South America. *J. Climate*, **22**, 300–315, https://doi.org/10.1175/2008JCLI2340.1.

Livezey, R. E., and W. Y. Chen, 1983: Statistical field significance and its determination by Monte Carlo techniques. *Mon. Wea. Rev.*, **111**, 46–59, https://doi.org/10.1175/1520-0493(1983)111<0046:SFSAID>2.0.CO;2.

Magaña, V., and M. Yanai, 1995: Mixed Rossby–gravity waves triggered by lateral forcing. *J. Atmos. Sci.*, **52**, 1473–1486, https://doi.org/10.1175/1520-0469(1995)052<1473:MRWTBL>2.0.CO;2.

Mak, M.-K., 1969: Laterally driven stochastic motions in the tropics. *J. Atmos. Sci.*, **26**, 41–64, https://doi.org/10.1175/1520-0469(1969)026<0041:LDSMIT>2.0.CO;2.

Matthews, A. J., 2021: Dynamical propagation and growth mechanisms for convectively coupled equatorial Kelvin waves over the Indian Ocean. *Quart. J. Roy. Meteor. Soc.*, **147**, 4310–4336, https://doi.org/10.1002/qj.4179.

——, and G. N. Kiladis, 1999a: Interactions between ENSO, transient circulation, and tropical convection over the Pacific. *J. Climate*, **12**, 3062–3086, https://doi.org/10.1175/1520-0442(1999)012<3062:IBETCA>2.0.CO;2.

——, and ——, 1999b: The tropical–extratropical interaction between high-frequency transients and the Madden–Julian oscillation. *Mon. Wea. Rev.*, **127**, 661–677, https://doi.org/10.1175/1520-0493(1999)127<0661:TTEIBH>2.0.CO;2.

——, and ——, 2000: A model of Rossby waves linked to submonthly convection over the eastern tropical Pacific. *J. Atmos. Sci.*, **57**, 3785–3798, https://doi.org/10.1175/1520-0469(2000)057<3785:AMORWL>2.0.CO;2.

Brought to you by NOAA Central Library | Unauthenticated | Downloaded 07/19/23 06:04 PM UTC

Mayta, V. C., G. N. Kiladis, J. Dias, P. L. S. Dias, and M. Gehne, 2021: Convectively coupled Kelvin waves over tropical South America. *J. Climate*, **34**, 6531–6547, https://doi.org/10.1175/JCLI-D-20-0662.1.

McGuirk, J. P., A. H. Thompson, and N. R. Smith, 1987: Moisture bursts over the tropical Pacific Ocean. *Mon. Wea. Rev.*, **115**, 787–798, https://doi.org/10.1175/1520-0493(1987)115<0787:MBOTTP>2.0.CO;2.

Ralph, F. M., P. J. Neiman, G. N. Kiladis, K. Weickmann, and D. W. Reynolds, 2011: A multiscale observational case study of a Pacific atmospheric river exhibiting tropical–extratropical connections and a mesoscale frontal wave. *Mon. Wea. Rev.*, **139**, 1169–1189, https://doi.org/10.1175/2010MWR3596.1.

Randel, W. J., and I. M. Held, 1991: Phase speed spectra of transient eddy fluxes and critical layer absorption. *J. Atmos. Sci.*, **48**, 688–697, https://doi.org/10.1175/1520-0469(1991)048<0688:PSSOTE>2.0.CO;2.

Ray, P., and C. Zhang, 2010: A case study of the mechanics of extratropical influence on the initiation of the Madden–Julian oscillation. *J. Atmos. Sci.*, **67**, 515–528, https://doi.org/10.1175/2009JAS3059.1.

Ren, P., D. Kim, M.-S. Ahn, D. Kang, and H.-L. Ren, 2021: Intercomparison of MJO column moist static energy and water vapor budget among six modern reanalysis products. *J. Climate*, **34**, 2977–3001, https://doi.org/10.1175/JCLI-D-20-0653.1.

Roundy, P. E., 2015: On the interpretation of EOF analysis of ENSO, atmospheric Kelvin waves, and the MJO. *J. Climate*, **28**, 1148–1165, https://doi.org/10.1175/JCLI-D-14-00398.1.

——, and W. M. Frank, 2004: A climatology of waves in the equatorial region. *J. Atmos. Sci.*, **61**, 2105–2132, https://doi.org/10.1175/1520-0469(2004)061<2105:ACOWIT>2.0.CO;2.

Ryoo, J.-M., Y. Kaspi, D. W. Waugh, G. N. Kiladis, D. E. Waliser, E. J. Fetzer, and J. Kim, 2013: Impact of Rossby wave breaking on U.S. west coast winter precipitation during ENSO events. *J. Climate*, **26**, 6360–6382, https://doi.org/10.1175/JCLI-D-12-00297.1.

Sakaeda, N., and P. E. Roundy, 2014: The role of interactions between multiscale circulations on the observed zonally averaged zonal wind variability associated with the Madden–Julian oscillation. *J. Atmos. Sci.*, **71**, 3816–3836, https://doi.org/10.1175/JAS-D-13-0304.1.

——, and ——, 2015: The development of upper-tropospheric wind over the Western Hemisphere in association with MJO convective initiation. *J. Atmos. Sci.*, **72**, 3138–3160, https://doi.org/10.1175/JAS-D-14-0293.1.

——, and ——, 2016: The development of upper-tropospheric geopotential height anomaly in the Western Hemisphere during MJO convective initiations. *Quart. J. Roy. Meteor. Soc.*, **142**, 942–956, https://doi.org/10.1002/qj.2696.

Sardeshmukh, P. D., and B. J. Hoskins, 1988: The generation of global rotational flow by steady idealized tropical divergence. *J. Atmos. Sci.*, **45**, 1228–1251, https://doi.org/10.1175/1520-0469(1988)045<1228:TGOGRF>2.0.CO;2.

Shapiro, M. A., H. Wernli, N. A. Bond, and R. Langland, 2001: The influence of the 1997–99 El Niño southern oscillation on extratropical baroclinic life cycles over the eastern North Pacific. *Quart. J. Roy. Meteor. Soc.*, **127**, 331–342, https://doi.org/10.1002/qj.49712757205.

Stan, C., D. M. Straus, J. S. Frederiksen, H. Lin, E. D. Maloney, and C. Schumacher, 2017: Review of tropical–extratropical teleconnections on intraseasonal time scales. *Rev. Geophys.*, **55**, 902–937, https://doi.org/10.1002/2016RG000538.

Straub, K. H., and G. N. Kiladis, 2002: Observations of a convectively coupled Kelvin wave in the eastern Pacific ITCZ. *J. Atmos. Sci.*, **59**, 30–53, https://doi.org/10.1175/1520-0469(2002)059<0030:OOACCK>2.0.CO;2.

——, and ——, 2003a: Extratropical forcing of convectively coupled Kelvin waves during austral winter. *J. Atmos. Sci.*, **60**, 526–543, https://doi.org/10.1175/1520-0469(2003)060<0526:EFOCCK>2.0.CO;2.

——, and ——, 2003b: The observed structure of convectively coupled Kelvin waves: Comparison with simple models of coupled wave instability. *J. Atmos. Sci.*, **60**, 1655–1668, https://doi.org/10.1175/1520-0469(2003)060<1655:TOSOCC>2.0.CO;2.

Straus, D. M., and R. S. Lindzen, 2000: Planetary-scale baroclinic instability and the MJO. *J. Atmos. Sci.*, **57**, 3609–3626, https://doi.org/10.1175/1520-0469(2000)057<3609:PSBIAT>2.0.CO;2.

Takayabu, Y. N., 1994: Large-scale cloud disturbances associated with equatorial waves. *J. Meteor. Soc. Japan*, **72**, 433–449, https://doi.org/10.2151/jmsj1965.72.3_433.

Thorncroft, C. D., B. J. Hoskins, and M. E. McIntyre, 1993: Two paradigms of baroclinic-wave life-cycle behaviour. *Quart. J. Roy. Meteor. Soc.*, **119**, 17–55, https://doi.org/10.1002/qj.49711950903.

Tomas, R. A., and P. J. Webster, 1994: Horizontal and vertical structure of cross-equatorial wave propagation. *J. Atmos. Sci.*, **51**, 1417–1430, https://doi.org/10.1175/1520-0469(1994)051<1417:HAVSOC>2.0.CO;2.

Tulich, S. N., and G. N. Kiladis, 2021: On the regionality of moist Kelvin waves and the MJO: The critical role of the background zonal flow. *J. Adv. Model. Earth Syst.*, **13**, e2021MS002528, https://doi.org/10.1029/2021MS002528.

Ventrice, M. J., C. D. Thorncroft, and M. A. Janiga, 2012: Atlantic tropical cyclogenesis: A three-way interaction between an African easterly wave, diurnally varying convection, and a convectively coupled atmospheric Kelvin wave. *Mon. Wea. Rev.*, **140**, 1108–1124, https://doi.org/10.1175/MWR-D-11-00122.1.

Wang, H., Y. Pan, A. Kumar, and W. Wang, 2013: Modulation of convectively coupled Kelvin wave activity in the tropical Pacific by ENSO. *J. Meteor. Res.*, **27**, 295–307, https://doi.org/10.1007/s13351-013-0306-5.

Wang, L., and L. Chen, 2016: Interannual variation of convectively-coupled equatorial waves and their association with environmental factors. *Dyn. Atmos. Oceans*, **76**, 116–126, https://doi.org/10.1016/j.dynatmoce.2016.10.004.

Webster, P. J., and J. R. Holton, 1982: Cross-equatorial response to middle-latitude forcing in a zonally varying basic state. *J. Atmos. Sci.*, **39**, 722–733, https://doi.org/10.1175/1520-0469(1982)039<0722:CERTML>2.0.CO;2.

Wheeler, M. C., and G. N. Kiladis, 1999: Convectively coupled equatorial waves: Analysis of clouds and temperature in the wavenumber–frequency domain. *J. Atmos. Sci.*, **56**, 374–399, https://doi.org/10.1175/1520-0469(1999)056<0374:CCEWAO>2.0.CO;2.

——, and H. H. Hendon, 2004: An all-season real-time multivariate MJO index: Development of an index for monitoring and prediction. *Mon. Wea. Rev.*, **132**, 1917–1932, https://doi.org/10.1175/1520-0493(2004)132<1917:AARMMI>2.0.CO;2.

Yanai, M., and M.-M. Lu, 1983: Equatorially trapped waves at the 200 mb level and their association with meridional convergence of wave energy flux. *J. Atmos. Sci.*, **40**, 2785–2803, https://doi.org/10.1175/1520-0469(1983)040<2785:ETWATM>2.0.CO;2.

Brought to you by NOAA Central Library | Unauthenticated | Downloaded 07/19/23 06:04 PM UTC

Yang, G.-Y., and B. J. Hoskins, 1996: Propagation of Rossby waves of nonzero frequency. *J. Atmos. Sci.*, **53**, 2365–2378, https://doi.org/10.1175/1520-0469(1996)053<2365:PORWON>2.0.CO;2.

——, and ——, 2013: ENSO impact on Kelvin waves and associated tropical convection. *J. Atmos. Sci.*, **70**, 3513–3532, https://doi.org/10.1175/JAS-D-13-081.1.

——, and ——, 2016: ENSO-related variation of equatorial MRG and Rossby waves and forcing from higher latitudes. *Quart. J. Roy. Meteor. Soc.*, **142**, 2488–2504, https://doi.org/10.1002/qj.2842.

——, ——, and J. Slingo, 2003: Convectively coupled equatorial waves: A new methodology for identifying wave structures in observational data. *J. Atmos. Sci.*, **60**, 1637–1654, https://doi.org/10.1175/1520-0469(2003)060<1637:CCEWAN>2.0.CO;2.

——, J. Methven, S. Woolnough, K. Hodges, and B. Hoskins, 2018: Linking African easterly wave activity with equatorial waves and the influence of Rossby waves from the Southern Hemisphere. *J. Atmos. Sci.*, **75**, 1783–1809, https://doi.org/10.1175/JAS-D-17-0184.1.

Ying, Y., and F. Zhang, 2017: Practical and intrinsic predictability of multiscale weather and convectively coupled equatorial waves during the active phase of an MJO. *J. Atmos. Sci.*, **74**, 3771–3785, https://doi.org/10.1175/JAS-D-17-0157.1.

Zangvil, A., and M. Yanai, 1980: Upper tropospheric waves in the tropics. Part I: Dynamical analysis in the wavenumber–frequency domain. *J. Atmos. Sci.*, **37**, 283–298, https://doi.org/10.1175/1520-0469(1980)037<0283:UTWITT>2.0.CO;2.

Zhang, C., 1993: Laterally forced equatorial perturbations in a linear model. Part II: Mobile forcing. *J. Atmos. Sci.*, **50**, 807–821, https://doi.org/10.1175/1520-0469(1993)050<0807:LFEPIA>2.0.CO;2.

——, and P. J. Webster, 1992: Laterally forced equatorial perturbations in a linear model. Part I: Stationary transient forcing. *J. Atmos. Sci.*, **49**, 585–607, https://doi.org/10.1175/1520-0469(1992)049<0585:LFEPIA>2.0.CO;2.

Brought to you by NOAA Central Library | Unauthenticated | Downloaded 07/19/23 06:04 PM UTC